

# Analysis of Linear Mode Connectivity via Permutation-Based Weight Matching

Akira Ito<sup>1</sup> Masanori Yamada<sup>1</sup> Atsutoshi Kumagai<sup>1</sup>

## Abstract

Recently, Ainsworth et al. (2023) showed that using weight matching (WM) to minimize the  $L_2$  distance in a permutation search of model parameters effectively identifies permutations that satisfy linear mode connectivity (LMC), in which the loss along a linear path between two independently trained models with different seeds remains nearly constant. This paper provides a theoretical analysis of LMC using WM, which is crucial for understanding stochastic gradient descent’s effectiveness and its application in areas like model merging. We first experimentally and theoretically show that permutations found by WM do not significantly reduce the  $L_2$  distance between two models and the occurrence of LMC is not merely due to distance reduction by WM in itself. We then provide theoretical insights showing that permutations can change the directions of the singular vectors, but not the singular values, of the weight matrices in each layer. This finding shows that permutations found by WM mainly align the directions of singular vectors associated with large singular values across models. This alignment brings the singular vectors with large singular values, which determine the model functionality, closer between pre-merged and post-merged models, so that the post-merged model retains functionality similar to the pre-merged models, making it easy to satisfy LMC. Finally, we analyze the difference between WM and straight-through estimator (STE), a dataset-dependent permutation search method, and show that WM outperforms STE, especially when merging three or more models.

<sup>1</sup>Nippon Telegraph and Telephone Corporation, 3–9–11 Midoricho, Musashino-shi, Tokyo, Japan. Correspondence to: Akira Ito <akira.itoh@ntt.com>.

## 1. Introduction

Deep learning has significantly advanced various fields, including image classification, speech recognition, and natural language processing (Vaswani et al., 2017; van den Oord et al., 2016; Zhao et al., 2023). Large-scale neural networks (NNs), such as Transformers, are widely used in these applications, and optimizing their parameters poses a massive non-convex optimization problem. Remarkably, stochastic gradient descent (SGD), which is widely used for training NNs, is known to find good solutions with high reproducibility despite its simplicity. One hypothesis for this seemingly counterintuitive phenomenon is that the landscape of the loss function may be much simpler than we previously thought. Recently, Garipov et al. (2018) have shown that SGD solutions are connected by simple curves where the loss values remain consistently low. Moreover, Entezari et al. (2022) conjectured that Conjecture 1.1 holds, considering all possible permutation symmetries of NNs:

**Conjecture 1.1** (Permutation invariance, informal). *Let  $\theta_a$  and  $\theta_b$  be any two SGD solutions (model parameters). Then, with high probability, there exists a permutation  $\pi$  such that the barrier (defined in Definition 2.1) between  $\theta_a$  and  $\pi(\theta_b)$  is sufficiently small.*

Here, the barrier represents the amount of increase in loss observed when linearly interpolating between the two models. Thus, a sufficiently small barrier implies that the model obtained by linear interpolation of the two models performs the same as the models before interpolation. If the barrier between two models is sufficiently small, we say linear mode connectivity (LMC) is satisfied between them (Frankle et al., 2020). Conjecture 1.1 suggests that most SGD solutions are part of the same loss basin by transferring each SGD solution to the same loss basin through permutations. Indeed, Ainsworth et al. (2023) demonstrated experimentally that this conjecture is valid for various datasets and models by using weight matching (WM), in which permutations are identified that minimize the  $L_2$  distance between the weights of the models.

The current theoretical analysis of why LMC occurs depends on the feasibility of closely matching NN weights using permutations. Recent work by Zhou et al. (2023) has proven that if the distance between the weights of two models can be sufficiently reduced through permutation, then LMC holds.

Intuitively, given two SGD solutions  $\theta_a$  and  $\theta_b$ , if one can find a permutation  $\pi$  such that  $\theta_a \approx \pi(\theta_b)$ , it is reasonable to expect that the outputs of the model corresponding to the interpolation between the two parameters  $\theta_a$  and  $\theta_b$  will be approximately equal to the outputs of the models  $\theta_a$  and  $\theta_b$ .

However, this paper reveals that this intuitive explanation is actually inaccurate and clarifies a more fundamental reason for why LMC holds through finding permutations by WM. The exploration of LMC principles is important not only to understand how SGD works in deep learning but also for its application in model merging (Ainsworth et al., 2023), where two independently trained models are combined. In particular, the method of finding permutations using only the  $L_2$  distance is versatile, dataset-independent, and computationally efficient. Therefore, the analysis in this study holds considerable potential for various applications such as model merging, federated learning, and continual learning.

The contributions of this paper are threefold:

**1. Demonstrating that WM does not make the  $L_2$  distance small enough that the two models can be considered approximately equal.** This paper experimentally demonstrates that permutations found by WM do not significantly reduce the  $L_2$  distance between two models. Specifically, even when distances are minimized using permutations, the resulting distance between two models is not sufficiently close to zero. Our results indicate that, even under LMC satisfaction, permutation reduces the model weight distance by no more than 20%. Our findings, supported by analysis based on a Taylor approximation, indicate that reducing the  $L_2$  distance by permutations is not in itself a reason to satisfy LMC.

**2. Revealing a reason for satisfying LMC by WM.** We provide both theoretical and experimental evidence showing that WM satisfies LMC by aligning the directions of singular vectors in the weights of each layer. First, we show that the singular values of each layer in a trained model do not vary significantly between models trained with different initializations. This indicates that the differences in the trained models arise not from the singular values, but from the directions of the singular vectors of each layer. Furthermore, we show both theoretically and experimentally that permutations found by WM align the directions of the singular vectors between two models. In particular, when minimizing the  $L_2$  distance, the directions of singular vectors with larger singular values are more likely to be aligned. By this singular-vector alignment, the singular vectors with large singular values, which determine the functionality of the model, become close between the pre-merged and post-merged models, so that the post-merged model has similar functionality to the pre-merged models, making it easy to satisfy LMC.

**3. Demonstrating the superiority of WM over the straight-through estimator (STE) in merging three or more models.** To see the difference between WM and other permutation search methods independent of  $L_2$  distance, we examine straight-through estimator (STE), which focuses on minimizing the barrier itself rather than the  $L_2$  distance. Our experiments reveal that permutations found by STE do not align the directions of singular vectors, highlighting a fundamental difference from WM in achieving LMC. In addition, we demonstrate experimentally that this difference has a significant impact on satisfying the LMC when merging three or more models.

## 2. Background and Preliminaries

### 2.1. Notation

For any natural number  $k \in \mathbb{N}$ , let  $[k] = \{1, 2, \dots, k\}$ . Bold uppercase variables represent tensors, including matrices (e.g.,  $\mathbf{X}$ ), and bold lowercase variables (e.g.,  $\mathbf{x}$ ) represent vectors. For any tensor  $\mathbf{X}$ , its vectorization is denoted by  $\text{vec}(\mathbf{X})$ . Throughout this paper,  $\|\mathbf{X}\|$  denotes the Frobenius ( $L_2$ ) norm of the tensor  $\mathbf{X}$ .

### 2.2. Permutation Invariance

We consider multilayer perceptrons (MLPs)  $f(\mathbf{x}; \theta)$  with  $L$  layers for simplicity while our analyses in this paper can be applied to any model architectures. Here,  $\mathbf{x} \in \mathbb{R}^{d_{\text{in}}}$  is the input to the NN, and  $\theta \in \mathbb{R}^{d_{\text{param}}}$  represents the model parameters, where  $d_{\text{in}} \in \mathbb{N}$  is the dimension of the input, and  $d_{\text{param}} \in \mathbb{N}$  is the dimension of the parameters. Let  $\mathbf{z}_\ell$  be the output of the  $\ell$ -th layer (i.e.,  $\mathbf{z}_0 = \mathbf{x}$ , and, for all  $\ell \in [L]$ ,  $\mathbf{z}_\ell = \sigma(\mathbf{W}_\ell \mathbf{z}_{\ell-1} + \mathbf{b}_\ell)$ ). Here,  $\sigma$  denotes the activation function, and  $\mathbf{W}_\ell$  and  $\mathbf{b}_\ell$  represent the weight and bias of the  $\ell$ -th layer, respectively. Note that in this MLP, we have  $\theta = \left\|_{\ell=1}^L (\text{vec}(\mathbf{W}_\ell) \parallel \mathbf{b}_\ell) \right\|$ , where  $\parallel$  represents the concatenation of vectors.

NNs have permutation symmetries of weight space. Considering an NN with model parameters  $\theta$ , for its  $\ell$ -th intermediate layer,

$$\mathbf{z}_\ell = \mathbf{P}^\top \mathbf{P} \mathbf{z}_\ell = \mathbf{P}^\top \sigma(\mathbf{P} \mathbf{W}_\ell \mathbf{z}_{\ell-1} + \mathbf{P} \mathbf{b}_\ell)$$

holds, where  $\mathbf{P}$  is a permutation matrix. Note that permutation matrices are orthogonal, so we have  $\mathbf{P}^\top = \mathbf{P}^{-1}$ . Therefore, by permuting the input of the  $(\ell+1)$ -st layer with  $\mathbf{P}^\top$ , the model parameters can be changed without altering the input-output relationship of the NN. Specifically, the new weights and bias are given by  $\mathbf{W}'_\ell = \mathbf{P} \mathbf{W}_\ell$ ,  $\mathbf{b}'_\ell = \mathbf{P} \mathbf{b}_\ell$ ,  $\mathbf{W}'_{\ell+1} = \mathbf{W}_{\ell+1} \mathbf{P}^\top$ . Such permutations can be applied to all layers. In this paper, we denote the tuple of permutations corresponding to each layer as  $\pi = (\mathbf{P}_\ell)_{\ell \in [L]}$ . Moreover, if a model  $\theta$  is given, the application of permutation  $\pi$  to  $\theta$  is denoted by  $\pi(\theta)$ .

### 2.3. Linear Mode Connectivity (LMC)

Let  $\theta \in \mathbb{R}^{d_{\text{param}}}$  be a model and  $\mathcal{L}(\theta)$  denote the value of the loss function for model  $\theta$ . Here, we define the loss barrier between two given models  $\theta_a$  and  $\theta_b$  as follows:

**Definition 2.1.** For two given models  $\theta_a$  and  $\theta_b$ , their loss barrier is defined as

$$B(\theta_a, \theta_b) := \max_{\lambda \in [0,1]} (\mathcal{L}(\lambda\theta_a + (1-\lambda)\theta_b) - (\lambda\mathcal{L}(\theta_a) + (1-\lambda)\mathcal{L}(\theta_b))).$$

Intuitively, the barrier represents the amount of increase in loss because of the linear interpolation of the two models. Two models  $\theta_a$  and  $\theta_b$  are said to be linearly mode connected when the loss barrier between them is approximately zero.

### 2.4. Permutation Selection

Entezari et al. (2022) conjectured that for any SGD solutions  $\theta_a$  and  $\theta_b$ , there exists a permutation  $\pi$  such that LMC holds between  $\theta_a$  and  $\pi(\theta_b)$  with high probability. Afterward, Ainsworth et al. (2023) proposed WM and STE as methods for finding such permutations. This subsection explains WM, the main focus of this paper. STE is discussed in Section 5.

In WM, we search for a permutation that minimizes the  $L_2$  distance between two models<sup>1</sup>:

$$\begin{aligned} \arg \min_{\pi} \|\theta_a - \pi(\theta_b)\|^2 \\ = \arg \min_{\pi} \sum_{\ell \in [L]} \|\mathbf{W}_{\ell}^{(a)} - P_{\ell} \mathbf{W}_{\ell}^{(b)} P_{\ell-1}^{\top}\|^2, \end{aligned} \quad (1)$$

where, without loss of generality, let  $P_L = \mathbf{I}$  and  $P_0 = \mathbf{I}$ , and  $\mathbf{I}$  is an identity matrix. This minimization problem is known as the sum of the bilinear assignments problem, which is NP-hard (Koopmans & Beckmann, 1957; Sahni & Gonzalez, 1976; Ainsworth et al., 2023). Therefore, Ainsworth et al. (2023) proposed a method to obtain an approximate solution by dividing the optimization for each layer separately and solving them individually. The divided optimization problem can be reduced to a simpler problem called the linear assignment problem, which can be easily solved using existing libraries like Scipy (Virtanen et al., 2020). Moreover, Peña et al. (2023) proposed solving Equation (1) using Sinkhorn’s algorithm (Adams & Zemel, 2011) by considering it as an optimal transport problem. This method allows optimization of all layers at once, potentially finding better solutions. Therefore, this paper adopts Sinkhorn’s algorithm-based method proposed in (Peña et al., 2023).

<sup>1</sup>Although only the weights are considered here, the biases can also be dealt with by concatenating the biases and the weights.

## 3. Motivating Observations

Previous studies have suggested that the closeness of two parameters in terms of  $L_2$  distance is critical for satisfying LMC. For example, Zhou et al. (2023) showed that LMC holds if a commutativity property is satisfied. This property holds if, for all layers  $\ell$ ,  $\mathbf{W}_{\ell}^{(a)} - P_{\ell} \mathbf{W}_{\ell}^{(b)} P_{\ell-1}^{\top} = \mathbf{0}$ . Zhou et al. (2023) argued in Section 5.2 that since WM finds the permutation that minimizes Equation (1), WM can be seen as searching for permutations that satisfy the commutativity property. In particular, there is a huge number of permutations because the total number of possible permutations grows exponentially as the number of layers and the width increase, and thus, some of them may sufficiently reduce the distance between the two models. However, this section explains from the perspective of a Taylor approximation that this intuition is not always correct. That is, our results demonstrate that even in cases where LMC is satisfied, the permutations found by WM do not necessarily bring the models as close as expected. The facts observed from the experiments in this section motivate us to explore other reasons for satisfying LMC in the following sections.

### 3.1. Closeness of Two Models in Terms of Taylor Approximation

This subsection demonstrates in terms of a second-order Taylor approximation that even with permutations found by WM, the distance between the two models is not close enough to be considered equal. Let  $\theta_a$  and  $\theta_b$  be two SGD solutions, and  $\pi$  be a permutation found by WM to make  $\pi(\theta_b)$  close to the model  $\theta_a$ . If the permutation brings  $\theta_a$  and  $\pi(\theta_b)$  sufficiently close, we can expect the Taylor approximation to hold on the loss function. Conversely, if the Taylor approximation does not hold, it means that  $\theta_a$  and  $\pi(\theta_b)$  are far enough apart that the approximation fails.

Let  $\theta_c = \lambda\theta_a + (1-\lambda)\pi(\theta_b)$  be the merged model at the ratio  $\lambda \in [0, 1]$ . If  $\theta_a$  and  $\pi(\theta_b)$  are sufficiently close, then their linear interpolation  $\theta_c$  should be close to both models. Therefore, the loss of the parameter  $\theta_c$  should be able to be approximated by the Taylor approximation. In fact, the following theorem holds if  $\theta_a$  and  $\pi(\theta_b)$  are sufficiently close:

**Theorem 3.1.** *The loss function  $\mathcal{L} : U \ni \theta \mapsto \mathcal{L}(\theta) \in \mathbb{R}$  is assumed to be a twice differentiable function on an open set  $U$  over  $\mathbb{R}^{d_{\text{param}}}$ . Let  $\mathbf{H}_a$  and  $\mathbf{H}_b$  be the Hessian matrices centered at the models  $\theta_a$  and  $\pi(\theta_b)$ , respectively. If, for any  $\lambda \in (0, 1)$ ,  $\lambda\theta_a + (1-\lambda)\pi(\theta_b) \in U$  holds, then we have*

$$\begin{aligned} B(\theta_a, \pi(\theta_b)) = \max_{\lambda} \lambda(1-\lambda) [\beta \boldsymbol{\mu}^{\top} \nabla (\mathcal{L}(\theta_a) - \mathcal{L}(\pi(\theta_b))) \\ + \frac{1}{2} \beta^2 \boldsymbol{\mu}^{\top} ((1-\lambda)\mathbf{H}_a + \lambda\mathbf{H}_b) \boldsymbol{\mu}] + O(\beta^3), \end{aligned} \quad (2)$$

where  $\nabla$  is the gradient with respect to the parameters, and

Table 1. Results of WM and the estimated value of barrier using Taylor approximation when  $\lambda = 1/2$ 

Dataset	Network	Barrier ( $\lambda = 1/2$ )	Taylor approx.	$L_2$ dist. w/o WM	$L_2$ dist. w/ WM
CIFAR10	VGG11	$0.035 \pm 0.1$	$2.956 \pm 0.35$	$799.503 \pm 16.396$	$746.465 \pm 19.576$
	ResNet20	$0.167 \pm 0.035$	$7.517 \pm 0.573$	$710.762 \pm 16.261$	$661.055 \pm 12.539$
FMNIST	MLP	$-0.183 \pm 0.049$	$0.928 \pm 0.175$	$121.853 \pm 5.83$	$100.041 \pm 4.71$
MNIST	MLP	$-0.033 \pm 0.006$	$0.036 \pm 0.03$	$81.231 \pm 5.58$	$64.751 \pm 4.795$

$O$  is the Landau symbol, and  $\mu$  is the unit vector from  $\theta_a$  to  $\pi(\theta_b)$  (i.e.,  $\mu = (\pi(\theta_b) - \theta_a) / \|\pi(\theta_b) - \theta_a\|$ ), and  $\beta$  represents the  $L_2$  distance between  $\theta_a$  and  $\pi(\theta_b)$ .

We prove this theorem in [Appendix B.1](#). The theorem states that if  $\theta_a$  and  $\pi(\theta_b)$  are sufficiently close, the value of the barrier can be predicted from the gradients and Hessian matrices around each model. In particular, when the distance  $\beta$  is small, the barrier tends to be close to zero regardless of the value of  $\lambda$ .

### 3.2. Experimental Results

We conducted experiments to empirically verify whether the Taylor approximation given by [Equation \(2\)](#) is a good approximation to estimate the barrier of two SGD solutions. [Table 1](#) shows the mean and standard deviation results from five trials of model merging (i.e., linear concatenation of the models  $(\theta_a + \pi(\theta_b))/2$ ). Details about the datasets, network training procedures, and permutation search methods used in these experiments are described in [Appendix C](#). The column labeled “Barrier” shows the value of the barrier at  $\lambda = 1/2$ . We choose  $\lambda = 1/2$  because it is empirically known that the midpoint between two models results in the highest loss ([Ainsworth et al., 2023; Peña et al., 2023](#)). Also, the approximation of [Equation \(2\)](#) at this point is shown in the column labeled “Taylor approx.” A negative value in the Barrier column indicates that the loss of the merged model is lower than the models before merging. As can be seen from the results, except for the MNIST dataset, there is a significant difference between the actual values of the barrier and those estimated by the Taylor approximation. These differences are particularly large for VGG11 and ResNet20. The table also shows the  $L_2$  distance between the models  $\theta_a$  and  $\theta_b$  before and after applying the permutation (i.e., “w/o WM” and “w/ WM”). The results show that the  $L_2$  distance changes by only about 6% to 20% from the original distance between  $\theta_a$  and  $\theta_b$ . This suggests that WM does not bring the models sufficiently close, at least not close enough for a second-order Taylor approximation to hold.

## 4. Analysis of LMC based on WM

This section explains why the permutation found by WM makes it possible to satisfy the LMC between the two models. First, [Section 4.1](#) shows that by performing singular

value decomposition (SVD) on the weight of each layer of the NN, the  $L_2$  distance between the two models can be expressed as the difference between the singular values and the singular vectors of the two models. Next, we show experimentally in [Section 4.2](#) that the distributions of the singular values are equal between independently trained models, indicating that the difference in weights between the models arises only from the difference in the singular vectors. We then show theoretically in [Section 4.3](#) that WM searches for permutations that match the directions of the singular vectors between the two models. In addition, we show experimentally in [Section 4.4](#) that the permutations obtained by WM cannot perfectly align the directions of all singular vectors of the models, and only singular vectors with large singular values can be aligned. Since the input-output relationship of a linear map induced from a matrix is approximately determined by its singular vectors with large singular values, the permutations obtained by WM are expected to play an important role in satisfying the LMC.

### 4.1. Analysis of WM Using SVD

The basic idea in analyzing WM is to perform an SVD of the weight in each layer. In WM, permutation matrices are searched for to minimize [Equation \(1\)](#). We denote the SVD of  $W_\ell^{(a)}$  and  $W_\ell^{(b)}$  by  $W_\ell^{(a)} = U_\ell^{(a)} S_\ell^{(a)} (V_\ell^{(a)})^\top = \sum_i u_{\ell,i}^{(a)} s_{\ell,i}^{(a)} (v_{\ell,i}^{(a)})^\top$  and  $W_\ell^{(b)} = U_\ell^{(b)} S_\ell^{(b)} (V_\ell^{(b)})^\top = \sum_j u_{\ell,j}^{(b)} s_{\ell,j}^{(b)} (v_{\ell,j}^{(b)})^\top$ , respectively. Here, we assume that the singular values are ordered in descending order (i.e., for all  $\ell \in [L]$ ,  $s_{\ell,1}^{(a)} \geq s_{\ell,2}^{(a)} \geq \dots \geq s_{\ell,n}^{(a)}$  and  $s_{\ell,1}^{(b)} \geq s_{\ell,2}^{(b)} \geq \dots \geq s_{\ell,n}^{(b)}$ ), where  $n$  is the number of singular values. Then, we have

$$\begin{aligned} \arg \min_{\pi} \|\theta_a - \pi(\theta_b)\|^2 \\ = \arg \min_{\pi} \sum_{\ell \in [L]} \left\| \sum_i u_{\ell,i}^{(a)} s_{\ell,i}^{(a)} (v_{\ell,i}^{(a)})^\top \right. \\ \left. - \sum_j P_\ell u_{\ell,j}^{(b)} s_{\ell,j}^{(b)} (P_{\ell-1} v_{\ell,j}^{(b)})^\top \right\|^2. \quad (3) \end{aligned}$$

[Equation \(3\)](#) shows that the permutation matrices  $P_\ell$  and  $P_{\ell-1}$  are multiplied by the left and right singular vectors of the model  $\theta_b$ , respectively. Since permutation matrices are orthogonal, the permutation matrices can change their



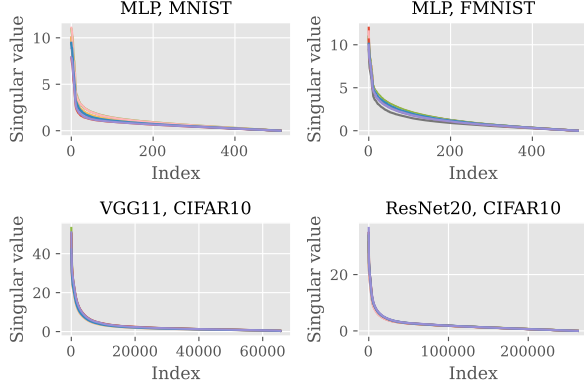


Figure 1. Distribution of the singular values of the second layer. The distribution of the singular values of all layers is shown in Appendix D.3.

directions, but not the norms, and therefore do not affect the magnitudes of the singular values. If the singular values of both models are almost equal (i.e., for all  $\ell$  and  $i$ ,  $s_{\ell,i}^{(a)} = s_{\ell,i}^{(b)}$ ) and we can find permutation matrices such that the left and right singular vectors of the two models match, then the two models  $\theta_a$  and  $\theta_b$  will be exactly the same. In other words, if one can match the singular values and singular vectors between the two models, then the LMC clearly holds. Therefore, in the following, we will discuss the differences in (1) singular values and (2) singular vectors of independently trained models.

#### 4.2. Difference Between Singular Values of Two Models

First, we investigate the differences between the singular values of two independently trained models. To this end, ten models are trained independently under identical conditions except for the seed, and their singular values are compared. Figure 1 plots the singular values in the second intermediate layer of independently trained models in descending order. The evaluation results for all the layers are shown in Figure 6. The singular values of ten independently trained models (i.e., trained with different seeds) are plotted in different colors. As can be seen in the figures, in the intermediate layers, the singular values are very close across all models.<sup>2</sup> Therefore, the differences in singular values between the models are not a major issue in achieving LMC.

#### 4.3. Role of Permutations in WM

We found that the distribution of singular values for each layer is approximately equal among independently trained

<sup>2</sup>As shown in Figure 6, there is some variation in the distribution of singular values in the final layer, but this is not a problem in terms of the test accuracy as described in Appendix D.2.

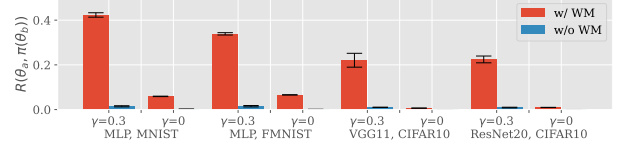


Figure 2. Evaluation results of singular vector alignment of  $\theta_a$  and  $\pi(\theta_b)$ .

models. Therefore, the differences between the models derive only from differences in the directions of the singular vectors.

Then, we show that WM finds the permutation matrices that align the singular vectors between two models. Specifically, the following theorem holds:

**Theorem 4.1.** *Given the trained  $L$ -layer MLPs  $\theta_a$  and  $\theta_b$ , Equation (3) is equivalent to*

$$\arg \max_{\pi=(P_\ell)_\ell} \sum_{\ell,i,j} s_{\ell,i}^{(a)} s_{\ell,j}^{(b)} (\mathbf{u}_{\ell,i}^{(a)})^\top (P_\ell \mathbf{u}_{\ell,j}^{(b)}) (\mathbf{v}_{\ell,i}^{(a)})^\top (P_{\ell-1} \mathbf{v}_{\ell,j}^{(b)}). \quad (4)$$

The proof of this theorem is shown in Appendix B.2. Focusing on the term for each layer  $\sum_{i,j} s_{\ell,i}^{(a)} s_{\ell,j}^{(b)} (\mathbf{u}_{\ell,i}^{(a)})^\top (P_\ell \mathbf{u}_{\ell,j}^{(b)}) (\mathbf{v}_{\ell,i}^{(a)})^\top (P_{\ell-1} \mathbf{v}_{\ell,j}^{(b)})$  in Equation (4),  $(\mathbf{u}_{\ell,i}^{(a)})^\top (P_\ell \mathbf{u}_{\ell,j}^{(b)})$  is the inner product between the left singular vector  $\mathbf{u}_{\ell,i}^{(a)}$  of the model  $\theta_a$  and the left singular vector  $\mathbf{u}_{\ell,j}^{(b)}$  of the model  $\theta_b$ , applied with the permutation matrix  $P_\ell$ . The permutation matrix is orthogonal, so it only permutes the elements without changing the norms of the left singular vectors. Therefore, this inner product is maximized when the directions of the two left singular vectors are aligned by the permutation matrix. Similarly,  $(\mathbf{v}_{\ell,i}^{(a)})^\top (P_{\ell-1} \mathbf{v}_{\ell,j}^{(b)})$  is the inner product of the right singular vectors, which is also maximized when the directions of the right singular vectors between two models are aligned by the permutation matrix  $P_{\ell-1}$ . Since these permutation matrices  $P_\ell$  and  $P_{\ell-1}$  are orthogonal, they do not change the norms of the vectors and thus do not affect the singular values  $s_{\ell,i}^{(a)}$  and  $s_{\ell,j}^{(b)}$ . Thus, Equation (4) is equivalent to finding permutation matrices that align the directions of the left and right singular vectors for all layers between two models, especially those corresponding to large singular values.

We have analyzed the MLPs, but as shown in Appendix A, almost the same holds for convolutional layers.

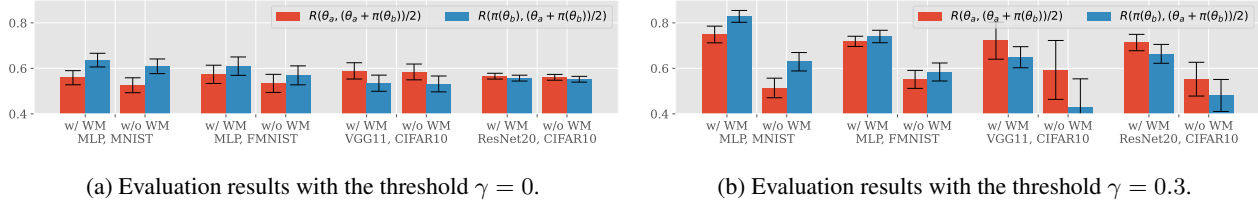


Figure 3. Evaluation results of WM between  $\theta_a$  and  $\theta_b$ . The blue bars represent the evaluation results of  $R$  between the model  $\theta_a$  and the merged model  $(\theta_a + \pi(\theta_b))/2$ , while the blue bars represent the evaluation results of  $R$  between the model  $\pi(\theta_b)$  and the merged model  $(\theta_a + \pi(\theta_b))/2$ .

#### 4.4. Experimental Validation of Singular-Vector Alignment

As already mentioned, the singular values are almost the same among independently trained models. Furthermore, the WM searches for permutations that minimize the difference between the singular vectors. If the WM can make the difference in singular vectors small enough, then the  $L_2$  distance between the two models also becomes almost zero, and the LMC is satisfied. However, as shown in Section 3, WM does not make the  $L_2$  distance very small. In other words, WM cannot perfectly align the directions of all singular vectors between the two models, and the number of singular vectors that can be changed in the direction by the WM is thought to be limited. Meanwhile, Theorem 4.1 shows that WM preferentially aligns the directions of singular vectors with large singular values. As shown in Figure 1, the singular vectors with large singular values are a small number of the total, so we expect that WM aligns the directions of only such dominant singular vectors. In this subsection, we experimentally confirm that this expectation is correct.

To evaluate how well the singular vectors are aligned, we calculate:

$$R(\theta_a, \pi(\theta_b)) = \frac{\sum_{\ell, i, j} (\mathbf{u}_{\ell, i}^{(a)})^\top \mathbf{P}_\ell \mathbf{u}_{\ell, j}^{(b)} (\mathbf{v}_{\ell, i}^{(a)})^\top \mathbf{P}_{\ell-1} \mathbf{v}_{\ell, j}^{(b)}}{\sum_\ell n_\ell}, \quad (5)$$

where  $n_\ell$  is the number of singular values in the  $\ell$ -th layer. Note that  $|R(\theta_a, \pi(\theta_b))| \leq 1$  holds and, we have equality if for all  $\ell$  and  $i$ ,  $\mathbf{u}_{\ell, i}^{(a)} = \mathbf{P}_\ell \mathbf{u}_{\ell, i}^{(b)}$  and  $\mathbf{v}_{\ell, i}^{(a)} = \mathbf{P}_{\ell-1} \mathbf{v}_{\ell, i}^{(b)}$  hold (proof in Appendix B.5). Therefore, if  $R(\theta_a, \pi(\theta_b))$  is close to one, the directions of the singular vectors of the models are aligned.

Figure 2 shows the results of evaluating Equation (5) between  $\theta_a$  and  $\pi(\theta_b)$ . The vertical axis in the figure represents the value of  $R$ . The red bars are the results when a permutation found by WM is applied to  $\theta_b$ , and the blue bars are the results when no permutations are applied. The figure shows the average and standard deviation of the results obtained from five permutation searches using WM.

In addition, a threshold  $\gamma$  is introduced to examine whether the singular vectors with the large singular values are preferentially aligned. For each model, we evaluate Equation (5) using only those whose ratio to the largest singular value is greater than  $\gamma$ . Thus,  $\gamma = 0$  in the figure corresponds to the results when all singular vectors are used, and  $\gamma = 0.3$  corresponds to the results when only singular values whose ratio to the largest singular value exceeds 0.3 are used.

The figure shows that the directions of the singular vectors are clearly more aligned with WM than without it. In particular, without WM, the value of  $R$  is almost zero, thus indicating that the singular vectors are nearly orthogonal. This would be related to the fact that the intermediate layer of the neural network is high-dimensional and random vectors on the high-dimensional space are orthogonal with high probability (Vershynin, 2018).

In addition, focusing on the difference in  $\gamma$ , when the singular vectors are aligned by using WM, the value of  $R$  is clearly larger when  $\gamma$  is 0.3. This means that singular vectors with larger singular values are aligned better. Although the value of  $R$  is not so large, especially around 0.2 at most for VGG11 and ResNet20, this singular vector alignment affects merged models.

Figure 3 shows the evaluation results of Equation (5) between the merged (i.e.,  $(\theta_a + \pi(\theta_b))/2$ ) and the pre-merged models (i.e.,  $\theta_a$  and  $\pi(\theta_b)$ ). If LMC holds, then the functionality of the post- and pre-merged models should be the same, which indicates that the directions of the singular vectors between these models should be close. To investigate how well the directions of singular vectors with large values are aligned between the post-merged and pre-merged models, we also show the results for  $\gamma = 0.3$  in Figure 3(b).

The figures show that when  $\gamma = 0$ , the value of  $R$  does not change much depending on whether WM is used or not, whereas when  $\gamma = 0.3$ , the value of  $R$  changes significantly depending on whether WM is used or not. This result indicates that the directions of singular vectors with particularly large singular values are aligned before and after the merge. The MLP results especially show that the value of  $R$  exceeds 0.7 by using WM. Since the input-output relationship

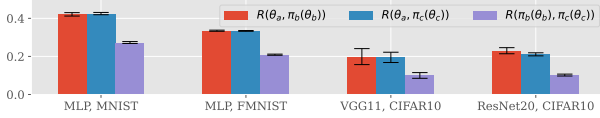


Figure 4. Evaluation results of  $R$  between each pair of the models with  $\gamma = 0.3$ .

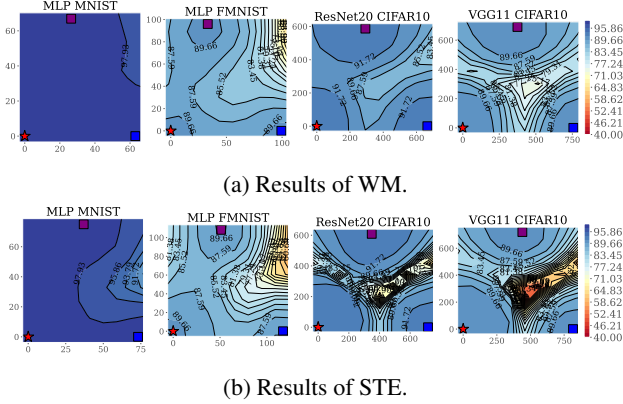


Figure 5. Accuracy landscape around  $\theta_a$ ,  $\pi_b(\theta_b)$  and  $\pi_c(\theta_c)$ . The star in the lower left represents  $\theta_a$ , and the squares in the lower right and upper represent  $\pi_b(\theta_b)$ , and  $\pi_c(\theta_c)$ , respectively.

of the linear map induced from the weight matrices of each layer is determined by the dominant singular vector with large singular values<sup>3</sup>, the function of the merged model should approach that of the model to be merged (i.e.,  $\theta_a$  and  $\theta_b$ ) by using WM, makes it easy to satisfy LMC.

The effect of changing model width on the singular-vector alignment by WM is discussed in Appendix D.3.

## 5. Comparison with STE

This section discusses the relationship between STE, a more direct method of finding permutation, and WM in terms of singular vectors. STE uses a dataset to find permutation matrices with a small barrier value. This section also explains that the STE and WM are based on essentially different principles, and shows that the difference has a significant impact on LMC among the three or more models.

<sup>3</sup>In fact, several papers (Choudhary et al., 2020; Sainath et al., 2013; Prabhavalkar et al., 2016) have been proposed to reduce the number of parameters without compromising performance by using low-rank approximation of NNs.

### 5.1. Straight-through Estimator (STE)

Ainsworth et al. (2023) proposed the STE, a permutation search method that finds a permutation  $\pi$  such that

$$\arg \min_{\pi} \mathcal{L} \left( \frac{1}{2} (\theta_a + \pi(\theta_b)) \right). \quad (6)$$

Since Equation (6) is difficult to solve directly, Ainsworth et al. (2023) proposed a method to decompose this optimization into a forward path to find permutations and a backward path to train the model obtained by the permutations found in the forward path, and to approximate the solution by iterating this process. In addition, Peña et al. (2023) proposed a method to solve Equation (6) directly using Sinkhorn’s algorithm. In this section, we adopt the latter method based on Sinkhorn’s algorithm, which we call STE in this paper. In the following subsections, we discuss the difference between the permutations found by STE and WM.

### 5.2. Experimental Results of Model Merging by STE

The results of model merging using STE are shown in Table 2. It also shows the  $L_2$  distance and the  $R$  value between the two models before and after the permutation, as well as Equation (2). Table 2 shows that despite the relatively small barrier value, the  $L_2$  distance between the two models before and after permutation hardly changes compared to the results with WM shown in Table 1. Since  $R(\theta_a, \pi(\theta_b))$  is nearly zero, the directions of the singular vectors between the two models are likely not aligned at all. Therefore, the reason for satisfying LMC by STE should be completely different from that of WM.

### 5.3. Merging Three Models

As shown in the previous subsection, the permutation matrices found by STE do not align the directions of the singular vectors of the models. This indicates that STE may find permutation matrices that reduce the loss of the merged model in a data-dependent manner (i.e., dependent on the loss landscape) rather than on the linear algebraic properties of the weight matrices of each layer. The difference between the principles of STE and WM could result in a qualitative difference in a model merging among three or more models.

Suppose we have three SGD solutions  $\theta_a$ ,  $\theta_b$ , and  $\theta_c$ . Let  $\pi_b$  and  $\pi_c$  be permutations that satisfy LMC between  $\theta_a$  and  $\pi_b(\theta_b)$ , and  $\theta_a$  and  $\pi_c(\theta_c)$ , respectively. If permutations found by STE depend on the locality of the loss landscape rather than the linear algebraic properties of the model weights, there is no guarantee that  $\pi_b(\theta_b)$  and  $\pi_c(\theta_c)$  are linearly mode-connected. In contrast, permutations found by WM align the directions of the singular vectors of the two models. In other words, the singular vectors of  $\pi_b(\theta_b)$

Table 2. Results of model merging with STE.

Dataset	Network	Barrier ( $\lambda = 1/2$ )	$L_2$ dist. w/o STE	$L_2$ dist. w/ STE	$R(\theta_a, \pi(\theta_b))$ ( $\gamma = 0.3$ )
CIFAR10	VGG11	$0.06 \pm 0.042$	$799.503 \pm 16.396$	$799.779 \pm 16.177$	$0.008 \pm 0.002$
	ResNet20	$0.119 \pm 0.119$	$710.762 \pm 16.261$	$711.142 \pm 16.048$	$0.005 \pm 0.004$
FMNIST	MLP	$-0.342 \pm 0.066$	$121.853 \pm 5.83$	$118.316 \pm 5.453$	$0.076 \pm 0.006$
MNIST	MLP	$-0.037 \pm 0.008$	$81.231 \pm 5.58$	$73.994 \pm 5.58$	$0.211 \pm 0.014$

and  $\pi_c(\theta_c)$  are also expected to be aligned. Thus, the LMC between  $\pi_b(\theta_b)$  and  $\pi_c(\theta_c)$  may not be satisfied in STE, while it is likely to be satisfied in WM.

We performed model merging experiments among three models to confirm the validity of the above discussion. First, Figure 4 presents the results of examining how well the singular vectors are aligned in each model by WM. Since the models  $\theta_b$  and  $\theta_c$  are matched to  $\theta_a$  through WM, it is expected that  $R(\theta_a, \pi_b(\theta_a))$  and  $R(\theta_a, \pi_c(\theta_c))$  would be large. On the other hand, although  $\theta_b$  and  $\theta_c$  were not explicitly made to approach each other,  $R(\pi_b(\theta_b), \pi_c(\theta_c))$  is clearly greater than zero, indicating that the directions of these two singular vectors are indirectly aligned by WM. From the result, the barrier between the models  $\pi_b(\theta_b)$  and  $\pi_c(\theta_c)$  is expected to be small. To confirm this, Figure 5 shows the test accuracy landscape around  $\theta_a$ ,  $\pi_b(\theta_b)$  and  $\pi_c(\theta_c)$ . The results of model merging at  $\lambda = 1/2$  for each pair of models are also shown in Table 3. Table 3 shows the mean and standard deviation of model merging three times. As can be seen from Figure 5, the barrier between  $\pi_b(\theta_b)$  and  $\pi_c(\theta_c)$  is smaller in WM than in STE. This means that there is a significant difference between the principles of permutations obtained by WM and STE. Figure 5 also shows that the landscape of test accuracy is flatter around the three models in WM than in STE. Therefore, WM is likely to be more advantageous, especially for merging more than or equal to three models.

## 6. Related Work

**(Linear) Mode Connectivity.** Several studies (Garipov et al., 2018; Draxler et al., 2018; Freeman & Bruna, 2017) have found that different NN solutions can be connected by nonlinear paths with almost no increase in loss. Nagarajan & Kolter (2019) first found that solutions can be connected by linear paths with an almost constant loss value in the case of training models on MNIST with the same random initial values. Later, Frankle et al. (2020) showed experimentally that LMC is not always satisfied between two SGD solutions, even with the same initial values, depending on the datasets and model architectures. However, they also showed that if a single model is trained for a certain period and then two models are trained independently from this pre-trained model as a starting point, they are linearly mode-connected. Furthermore, Frankle et al. (2020) showed the relationship between LMC and the lottery-ticket

hypothesis (Frankle & Carbin, 2019). Entezari et al. (2022) conjectured that LMC is satisfied with a high probability between two SGD solutions by taking into account the permutation symmetries in the hidden layers. Then, Ainsworth et al. (2023) proposed a WM method by formulating the neuron alignment as a bipartite graph matching problem and solving it approximately. Afterward, Peña et al. (2023) proposed using Sinkhorn’s algorithm to solve the WM directly. While several papers (Venturi et al., 2019; Nguyen et al., 2019; Nguyen, 2019; Kuditipudi et al., 2019) have discussed non-linear mode connectivity, there is little theoretical analysis in LMC. Zhou et al. (2023) introduced the concept of layerwise linear feature connectivity (LLFC) and showed that LLFC implies LMC. Also, Zhou et al. (2023) showed that if the ReLU function is approximately linear (weak additivity for ReLU activation) and the commutativity property is satisfied, then LLFC and LMC are also satisfied. However, we show that the  $L_2$  distance between the models after permutation is not close enough to satisfy the commutativity property. This fact motivated us to investigate the relationship between LMC and WM.

**Model Merging.** LMC is a property related to merging two models, so its relevant topics include model merging and federated learning. McMahan et al. (2017); Konečný et al. (2016) introduced the concept of federated learning, where a model is trained on divided datasets. Wang et al. (2020) proposed a method for federated learning by permuting each component unit and then averaging the weights of the models. Singh & Jaggi (2020) proposed a method for merging models by performing a soft alignment of model weights using optimal transport, which is very similar to the method proposed by Zhou et al. (2023). Wortsman et al. (2022) proposed a method to improve test accuracy without increasing inference cost, unlike ensemble methods, by averaging the weights of models fine-tuned with different hyperparameters.

## 7. Conclusion

This paper analyzed why linear mode connectivity (LMC) is satisfied by permutation search with weight matching (WM). First, we showed that WM does not reduce the distance between the weights of two models as much as previously thought, and then we analyzed WM in terms of singular value decomposition. Our analysis showed that WM has the



effect of aligning the directions of singular vectors with large singular values, which plays an important role in achieving LMC. Finally, we compared WM with straight-through estimator (STE), a dataset-dependent permutation search method, and showed that WM is superior at merging three or more models.

## Potential Broader Impact

This paper presents work whose goal is to advance the field of Machine Learning. There are many potential societal consequences of our work, none which we feel must be specifically highlighted here.

## References

- Adams, R. P. and Zemel, R. S. Ranking via sinkhorn propagation, 2011.
- Ainsworth, S., Hayase, J., and Srinivasa, S. Git re-basin: Merging models modulo permutation symmetries. In *The Eleventh International Conference on Learning Representations*, 2023. URL <https://openreview.net/forum?id=CQsmMYmlP5T>.
- Choudhary, T., Mishra, V., Goswami, A., and Sarangapani, J. A comprehensive survey on model compression and acceleration. *Artificial Intelligence Review*, 53(7):5113–5155, Oct 2020. ISSN 1573-7462. doi: 10.1007/s10462-020-09816-7. URL <https://doi.org/10.1007/s10462-020-09816-7>.
- Draxler, F., Veschgini, K., Salmhofer, M., and Hamprecht, F. Essentially no barriers in neural network energy landscape. In Dy, J. and Krause, A. (eds.), *Proceedings of the 35th International Conference on Machine Learning*, volume 80 of *Proceedings of Machine Learning Research*, pp. 1309–1318. PMLR, 10–15 Jul 2018. URL <https://proceedings.mlr.press/v80/draxler18a.html>.
- Entezari, R., Sedghi, H., Saukh, O., and Neyshabur, B. The role of permutation invariance in linear mode connectivity of neural networks, 2022.
- Frankle, J. and Carbin, M. The lottery ticket hypothesis: Finding sparse, trainable neural networks. In *International Conference on Learning Representations*, 2019. URL <https://openreview.net/forum?id=rJl-b3RcF7>.
- Frankle, J., Dziugaite, G. K., Roy, D., and Carbin, M. Linear mode connectivity and the lottery ticket hypothesis. In III, H. D. and Singh, A. (eds.), *Proceedings of the 37th International Conference on Machine Learning*, volume 119 of *Proceedings of Machine Learning Research*, pp. 3259–3269. PMLR, 13–18 Jul 2020. URL <https://proceedings.mlr.press/v119/frankle20a.html>.
- Freeman, C. D. and Bruna, J. Topology and geometry of half-rectified network optimization. In *International Conference on Learning Representations*, 2017. URL <https://openreview.net/forum?id=Bk0FWVcgx>.
- Garipov, T., Izmailov, P., Podoprikin, D., Vetrov, D. P., and Wilson, A. G. Loss surfaces, mode connectivity, and fast ensembling of dnns. In Bengio, S., Wallach, H., Larochelle, H., Grauman, K., Cesa-Bianchi, N., and Garnett, R. (eds.), *Advances in Neural Information Processing Systems*, volume 31. Curran Associates, Inc., 2018. URL [https://proceedings.neurips.cc/paper\\_files/paper/2018/file/be3087e74e9100d4bc4c6268cdbc8456-Paper.pdf](https://proceedings.neurips.cc/paper_files/paper/2018/file/be3087e74e9100d4bc4c6268cdbc8456-Paper.pdf).
- Goodfellow, I., Bengio, Y., and Courville, A. *Deep Learning*. MIT Press, 2016. <http://www.deeplearningbook.org>.
- Jain, A. K. *Fundamentals of digital image processing*. Prentice-Hall, Inc., USA, 1989. ISBN 0133361659.
- Jordan, K., Sedghi, H., Saukh, O., Entezari, R., and Neyshabur, B. REPAIR: RENormalizing permuted activations for interpolation repair. In *The Eleventh International Conference on Learning Representations*, 2023. URL <https://openreview.net/forum?id=gU5sJ6ZggcX>.
- Konečný, J., McMahan, H. B., Ramage, D., and Richtárik, P. Federated optimization: Distributed machine learning for on-device intelligence, 2016.
- Koopmans, T. C. and Beckmann, M. Assignment problems and the location of economic activities. *Econometrica*, 25(1):53–76, 1957. ISSN 00129682, 14680262. URL <http://www.jstor.org/stable/1907742>.
- Kuditipudi, R., Wang, X., Lee, H., Zhang, Y., Li, Z., Hu, W., Ge, R., and Arora, S. Explaining landscape connectivity of low-cost solutions for multilayer nets. In Wallach, H., Larochelle, H., Beygelzimer, A., d’Alché-Buc, F., Fox, E., and Garnett, R. (eds.), *Advances in Neural Information Processing Systems*, volume 32. Curran Associates, Inc., 2019. URL [https://proceedings.neurips.cc/paper\\_files/paper/2019/file/46a4378f835dc8040c8057beb6a2da52-Paper.pdf](https://proceedings.neurips.cc/paper_files/paper/2019/file/46a4378f835dc8040c8057beb6a2da52-Paper.pdf).
- McMahan, B., Moore, E., Ramage, D., Hampson, S., and Arcas, B. A. y. Communication-Efficient Learning of Deep Networks from Decentralized Data. In

- Singh, A. and Zhu, J. (eds.), *Proceedings of the 20th International Conference on Artificial Intelligence and Statistics*, volume 54 of *Proceedings of Machine Learning Research*, pp. 1273–1282. PMLR, 20–22 Apr 2017. URL <https://proceedings.mlr.press/v54/mcmahan17a.html>.
- Nagarajan, V. and Kolter, J. Z. Uniform convergence may be unable to explain generalization in deep learning. In Wallach, H., Larochelle, H., Beygelzimer, A., d'Alché-Buc, F., Fox, E., and Garnett, R. (eds.), *Advances in Neural Information Processing Systems*, volume 32. Curran Associates, Inc., 2019. URL [https://proceedings.neurips.cc/paper\\_files/paper/2019/file/05e97c207235d63ceb1db43c60db7bbb-Paper.pdf](https://proceedings.neurips.cc/paper_files/paper/2019/file/05e97c207235d63ceb1db43c60db7bbb-Paper.pdf).
- Nguyen, Q. On connected sublevel sets in deep learning. In Chaudhuri, K. and Salakhutdinov, R. (eds.), *Proceedings of the 36th International Conference on Machine Learning*, volume 97 of *Proceedings of Machine Learning Research*, pp. 4790–4799. PMLR, 09–15 Jun 2019. URL <https://proceedings.mlr.press/v97/nguyen19a.html>.
- Nguyen, Q., Mukkamala, M. C., and Hein, M. On the loss landscape of a class of deep neural networks with no bad local valleys. In *International Conference on Learning Representations*, 2019. URL <https://openreview.net/forum?id=HJgXsjA5tQ>.
- Peña, F. A. G., Medeiros, H. R., Dubail, T., Aminbeidokhti, M., Granger, E., and Pedersoli, M. Re-basin via implicit sinkhorn differentiation. In *Proceedings of the IEEE/CVF Conference on Computer Vision and Pattern Recognition (CVPR)*, pp. 20237–20246, June 2023.
- Prabhavalkar, R., Alsharif, O., Bruguier, A., and McGraw, L. On the compression of recurrent neural networks with an application to lvcsr acoustic modeling for embedded speech recognition. In *2016 IEEE International Conference on Acoustics, Speech and Signal Processing (ICASSP)*, pp. 5970–5974, 2016. doi: 10.1109/ICASSP.2016.7472823.
- Sahni, S. and Gonzalez, T. P-complete approximation problems. *J. ACM*, 23(3):555–565, jul 1976. ISSN 0004-5411. doi: 10.1145/321958.321975. URL <https://doi.org/10.1145/321958.321975>.
- Sainath, T. N., Kingsbury, B., Sindhvani, V., Arisoy, E., and Ramabhadran, B. Low-rank matrix factorization for deep neural network training with high-dimensional output targets. In *2013 IEEE International Conference on Acoustics, Speech and Signal Processing*, pp. 6655–6659, 2013. doi: 10.1109/ICASSP.2013.6638949.
- Sedghi, H., Gupta, V., and Long, P. M. The singular values of convolutional layers. In *International Conference on Learning Representations*, 2019. URL <https://openreview.net/forum?id=rJevYoA9Fm>.
- Singh, S. P. and Jaggi, M. Model fusion via optimal transport. In Larochelle, H., Ranzato, M., Hadsell, R., Balcan, M., and Lin, H. (eds.), *Advances in Neural Information Processing Systems*, volume 33, pp. 22045–22055. Curran Associates, Inc., 2020. URL [https://proceedings.neurips.cc/paper\\_files/paper/2020/file/fb2697869f56484404c8ceee2985b01d-Paper.pdf](https://proceedings.neurips.cc/paper_files/paper/2020/file/fb2697869f56484404c8ceee2985b01d-Paper.pdf).
- van den Oord, A., Dieleman, S., Zen, H., Simonyan, K., Vinyals, O., Graves, A., Kalchbrenner, N., Senior, A., and Kavukcuoglu, K. Wavenet: A generative model for raw audio, 2016.
- Vaswani, A., Shazeer, N., Parmar, N., Uszkoreit, J., Jones, L., Gomez, A. N., Kaiser, L. u., and Polosukhin, I. Attention is all you need. In Guyon, I., Luxburg, U. V., Bengio, S., Wallach, H., Fergus, R., Vishwanathan, S., and Garnett, R. (eds.), *Advances in Neural Information Processing Systems*, volume 30. Curran Associates, Inc., 2017. URL [https://proceedings.neurips.cc/paper\\_files/paper/2017/file/3f5ee243547dee91fbd053c1c4a845aa-Paper.pdf](https://proceedings.neurips.cc/paper_files/paper/2017/file/3f5ee243547dee91fbd053c1c4a845aa-Paper.pdf).
- Venturi, L., Bandeira, A. S., and Bruna, J. Spurious valleys in one-hidden-layer neural network optimization landscapes. *Journal of Machine Learning Research*, 20(133): 1–34, 2019. URL <http://jmlr.org/papers/v20/18-674.html>.
- Vershynin, R. *High-Dimensional Probability: An Introduction with Applications in Data Science*. Number 47 in Cambridge Series in Statistical and Probabilistic Mathematics. Cambridge University Press, 2018. ISBN 978-1-108-41519-4.
- Virtanen, P., Gommers, R., Oliphant, T. E., Haberland, M., Reddy, T., Cournapeau, D., Burovski, E., Peterson, P., Weckesser, W., Bright, J., van der Walt, S. J., Brett, M., Wilson, J., Millman, K. J., Mayorov, N., Nelson, A. R. J., Jones, E., Kern, R., Larson, E., Carey, C. J., Polat, İ., Feng, Y., Moore, E. W., VanderPlas, J., Laxalde, D., Perktold, J., Cimrman, R., Henriksen, I., Quintero, E. A., Harris, C. R., Archibald, A. M., Ribeiro, A. H., Pedregosa, F., van Mulbregt, P., and SciPy 1.0 Contributors. SciPy 1.0: Fundamental Algorithms for Scientific Computing in Python. *Nature Methods*, 17:261–272, 2020. doi: 10.1038/s41592-019-0686-2.

von Neumann, J. Some matrix-inequalities and metrization of matrix-space tomsk univ. rev., 1 (1937), 1962.

Wang, H., Yurochkin, M., Sun, Y., Papailiopoulos, D., and Khazaeni, Y. Federated learning with matched averaging. In *International Conference on Learning Representations*, 2020. URL <https://openreview.net/forum?id=BkluqlSFDS>.

Wortsman, M., Ilharco, G., Gadre, S. Y., Roelofs, R., Gontijo-Lopes, R., Morcos, A. S., Namkoong, H., Farhadi, A., Carmon, Y., Kornblith, S., and Schmidt, L. Model soups: averaging weights of multiple fine-tuned models improves accuracy without increasing inference time. In Chaudhuri, K., Jegelka, S., Song, L., Szepesvari, C., Niu, G., and Sabato, S. (eds.), *Proceedings of the 39th International Conference on Machine Learning*, volume 162 of *Proceedings of Machine Learning Research*, pp. 23965–23998. PMLR, 17–23 Jul 2022. URL <https://proceedings.mlr.press/v162/wortsman22a.html>.

Zhao, W. X., Zhou, K., Li, J., Tang, T., Wang, X., Hou, Y., Min, Y., Zhang, B., Zhang, J., Dong, Z., Du, Y., Yang, C., Chen, Y., Chen, Z., Jiang, J., Ren, R., Li, Y., Tang, X., Liu, Z., Liu, P., Nie, J.-Y., and Wen, J.-R. A survey of large language models, 2023.

Zhou, Z., Yang, Y., Yang, X., Yan, J., and Hu, W. Going beyond linear mode connectivity: The layerwise linear feature connectivity. In *Thirty-seventh Conference on Neural Information Processing Systems*, 2023. URL <https://openreview.net/forum?id=vORUhrVEnH>.

## A. Convolutional Layers

This section proves the theorem like [Theorem 4.1](#) holds for convolutional neural networks (CNNs).

### A.1. Notation

We introduce the notation used in the following sections. Each element of a tensor is specified by a simple italic variable with subscripts (e.g., for a third-order tensor  $\mathbf{X}$ , its  $i, j, k$ -th component is denoted by  $X_{i,j,k}$ ). In this paper, we also use Python-like slice notation. For example,  $\mathbf{X}_{1,:}$  denotes the first row of the matrix  $\mathbf{X}$ . For a complex matrix  $\mathbf{X}$ , let  $\mathbf{X}^* = \overline{\mathbf{X}}^\top$  be its unitary transpose, where  $\overline{\mathbf{X}}$  denotes the complex conjugate of  $\mathbf{X}$ .

### A.2. Matrix Representation of Convolutional Layer

This subsection introduces the matrix representation of a convolutional layer. Let  $\mathbf{X} \in \mathbb{R}^{m \times n \times n}$  and  $\mathbf{Y} \in \mathbb{R}^{m \times n \times n}$  be the input and the output of the  $\ell$ -th convolutional layer, respectively, where  $m$  denotes the number of input and output channels and  $n$  denotes the size of height and width of the input. Although we assume that the numbers of output channels and input channels are identical and the sizes of the height and width of the input are also identical for simplicity, our analysis can be applicable even when they are not identical. Let  $\mathbf{K} \in \mathbb{R}^{n \times n \times m \times m}$  be the kernel of the  $\ell$ -th layer. Then we have

$$Y_{c,r,i} = \sum_{d \in [m], p \in [n], q \in [n]} X_{d,r+p,i+q} K_{p,q,c,d}.$$

Here, there exists a matrix  $\mathbf{M}$  such that  $\text{vec}(\mathbf{Y}) = \mathbf{M} \text{vec}(\mathbf{X})$  holds ([Sedghi et al., 2019](#); [Jain, 1989](#); [Goodfellow et al., 2016](#)), where

$$\mathbf{M} = \begin{pmatrix} \mathbf{B}_{1,1} & \mathbf{B}_{1,2} & \cdots & \mathbf{B}_{1,m} \\ \mathbf{B}_{2,1} & \mathbf{B}_{2,2} & \cdots & \mathbf{B}_{2,m} \\ \vdots & \vdots & \ddots & \vdots \\ \mathbf{B}_{m,1} & \mathbf{B}_{m,2} & \cdots & \mathbf{B}_{m,m} \end{pmatrix}. \quad (7)$$

Here for all  $c, d \in [m]$ ,  $\mathbf{B}_{c,d}$  is a doubly circulant matrix defined by

$$\mathbf{B}_{c,d} = \begin{pmatrix} \text{circ}(K_{1,:,c,d}) & \text{circ}(K_{2,:,c,d}) & \cdots & \text{circ}(K_{n,:,c,d}) \\ \text{circ}(K_{n,:,c,d}) & \text{circ}(K_{1,:,c,d}) & \cdots & \text{circ}(K_{n-1,:,c,d}) \\ \vdots & \vdots & \ddots & \vdots \\ \text{circ}(K_{2,:,c,d}) & \text{circ}(K_{3,:,c,d}) & \cdots & \text{circ}(K_{1,:,c,d}) \end{pmatrix},$$

where  $\text{circ}$  is a function to generate a circulant matrix from a given vector. For example, given a vector  $\mathbf{a} = (a_1, a_2, \dots, a_3)$ ,

the circulant matrix generated by  $\mathbf{a}$  is given by  $\text{circ}(\mathbf{a}) = \begin{pmatrix} a_1 & a_2 & a_3 \\ a_3 & a_1 & a_2 \\ a_2 & a_3 & a_1 \end{pmatrix}$ .

### A.3. Singular Value Decomposition and Weight Matching of Convolutional Layer

Since [Equation \(7\)](#) represents the matrix form of the convolutional layer, we can reach a similar conclusion to [Theorem 4.1](#) by performing a singular value decomposition (SVD) on it. However, as this matrix is a huge matrix of size  $mn^2 \times mn^2$ , directly performing an SVD is not practical. Therefore, we decompose it into a more SVD-friendly form by applying a Fourier transform. Using the imaginary unit as  $\eta = \sqrt{-1}$ , and setting  $\omega = e^{-2\pi\eta/n}$ , a one-dimensional Fourier transform matrix  $\mathbf{F}$  is defined by  $F_{i,j} = (\omega^{(i-1)(j-1)})_{i,j}$ .<sup>4</sup> A matrix corresponding to the two-dimensional Fourier transform can be defined as  $\mathbf{Q} = (\mathbf{F} \otimes \mathbf{F}^*)/n$ . Here,  $\otimes$  denotes the Kronecker product, and  $\mathbf{F}^*$  represents the unitary transpose of the matrix  $\mathbf{F}$ . By using this two-dimensional Fourier transform matrix  $\mathbf{Q}$ , the matrix  $\mathbf{M}$  can be decomposed as follows:

$$\mathbf{M} = (\mathbf{I}_m \otimes \mathbf{Q})^* \mathbf{L} (\mathbf{I}_m \otimes \mathbf{Q}),$$

<sup>4</sup>Usually, the alphabet letters  $i$  or  $j$  are used for the imaginary unit, but since they are used as indices here, we conveniently use  $\eta$ .



where  $\mathbf{I}_m$  denotes the identity matrix with size of  $m \times m$ , and we have

$$\mathbf{L} = \begin{pmatrix} \mathbf{D}_{1,1} & \mathbf{D}_{1,2} & \cdots & \mathbf{D}_{1,m} \\ \mathbf{D}_{2,1} & \mathbf{D}_{2,2} & \cdots & \mathbf{D}_{2,m} \\ \vdots & \vdots & \ddots & \vdots \\ \mathbf{D}_{m,1} & \mathbf{D}_{m,2} & \cdots & \mathbf{D}_{m,m} \end{pmatrix}.$$

Here, for all  $c, d \in [m]$ ,  $\mathbf{D}_{c,d} = \mathbf{Q}\mathbf{B}_{c,d}\mathbf{Q}^*$  is a complex diagonal matrix (Sedghi et al., 2019). Let  $\mathbf{G}_{:,w}$  be a matrix formed by extracting the  $w$ -th diagonal element of each diagonal matrix  $\mathbf{D}_{c,d}$  and arranging them (i.e.,  $\mathbf{G}_{c,d,w} = (\mathbf{D}_{c,d})_{w,w}$ ). Then, the following theorem holds:

**Theorem A.1** (SVD of convolutional layer). *Let  $s_{w,i}$ ,  $\mathbf{u}_{w,i}$ , and  $\mathbf{v}_{w,i}$  be the  $i$ -th singular value, left singular vector, and right singular vector of  $\mathbf{G}_{:,w}$ , respectively. Then, the matrix  $\mathbf{M}$  representing the convolutional layer can be decomposed as follows:*

$$\mathbf{M} = \sum_{w,i} (\mathbf{u}_{w,i} \otimes \mathbf{Q}\mathbf{e}_w) s_{w,i} (\mathbf{v}_{w,i} \otimes \mathbf{Q}\mathbf{e}_w)^*,$$

where  $\mathbf{e}_w$  represents the orthonormal basis in Euclidean space  $\mathbb{R}^{n^2}$ , and  $s_{w,i}$ ,  $\mathbf{u}_{w,i} \otimes \mathbf{Q}\mathbf{e}_w$ , and  $\mathbf{v}_{w,i} \otimes \mathbf{Q}\mathbf{e}_w$  are the singular value, left singular vector, and right singular vector of  $\mathbf{M}$ , respectively.

The proof is shown in Appendix B.3. From this theorem, the following theorem can be proved:

**Theorem A.2.** *Let  $\mathbf{M}^{(a)}$  and  $\mathbf{M}^{(b)}$  be the matrix representations of convolutional layers of two CNNs. From Theorem A.1, their SVDs are given by  $\mathbf{M}^{(a)} = \sum_{w,i} (\mathbf{u}_{w,i}^{(a)} \otimes \mathbf{Q}\mathbf{e}_w) s_{w,i}^{(a)} (\mathbf{v}_{w,i}^{(a)} \otimes \mathbf{Q}\mathbf{e}_w)^*$  and  $\mathbf{M}^{(b)} = \sum_{w,i} (\mathbf{u}_{w,i}^{(b)} \otimes \mathbf{Q}\mathbf{e}_w) s_{w,i}^{(b)} (\mathbf{v}_{w,i}^{(b)} \otimes \mathbf{Q}\mathbf{e}_w)^*$ , respectively. Then, the WM between  $\mathbf{M}^{(a)}$  and  $\mathbf{M}^{(b)}$  is equivalent to finding permutation matrices  $\mathbf{P}_\ell$  and  $\mathbf{P}_{\ell-1}$  such that*

$$\arg \max_{\mathbf{P}_\ell, \mathbf{P}_{\ell-1}} \Re \sum_{w,i,j} s_{w,i}^{(a)} s_{w,j}^{(b)} \overline{(\mathbf{u}_{w,i}^{(a)})^* (\mathbf{P}_\ell \mathbf{u}_{w,j}^{(b)})} (\mathbf{v}_{w,i}^{(a)})^* (\mathbf{P}_{\ell-1} \mathbf{v}_{w,j}^{(b)}),$$

where  $\Re z$  is the real part of  $z$  for a complex number  $z$ .

The proof is shown in Appendix B.4. Similar to the case of MLP (Theorem 4.1), Theorem A.2 indicates that WM has the effect of aligning the directions of the corresponding singular vectors in convolutional layers.

## B. Proofs

### B.1. Proof of Theorem 3.1

*Proof.* From the assumption and Taylor theorem centered at  $\theta_a$ , we have

$$\begin{aligned} \mathcal{L}(\theta_c) &= \mathcal{L}(\theta_a) + (\theta_c - \theta_a)^\top \nabla \mathcal{L}(\theta_a) + \frac{1}{2} (\theta_c - \theta_a)^\top \mathbf{H}_a (\theta_c - \theta_a) + O(\|\theta_c - \theta_a\|^3) \\ &= \mathcal{L}(\theta_a) + (1 - \lambda) \beta \mu^\top \nabla \mathcal{L}(\theta_a) + \frac{1}{2} (1 - \lambda)^2 \beta^2 \mu^\top \mathbf{H}_a \mu + O(\beta^3). \end{aligned}$$

Similarly, using Taylor theorem centered at  $\pi(\theta_b)$ , we get

$$\begin{aligned} \mathcal{L}(\theta_c) &= \mathcal{L}(\pi(\theta_b)) + (\theta_c - \pi(\theta_b))^\top \nabla \mathcal{L}(\pi(\theta_b)) + \frac{1}{2} (\theta_c - \pi(\theta_b))^\top \mathbf{H}_a (\theta_c - \pi(\theta_b)) + O(\|\theta_c - \pi(\theta_b)\|^3) \\ &= \mathcal{L}(\pi(\theta_b)) - \lambda \beta \mu^\top \nabla \mathcal{L}(\pi(\theta_b)) + \frac{1}{2} \lambda^2 \beta^2 \mu^\top \mathbf{H}_a \mu + O(\beta^3). \end{aligned}$$

Combining these equations, the barrier can be obtained as

$$\begin{aligned} B(\theta_a, \pi(\theta_b)) &= \max_{\lambda} (\mathcal{L}(\theta_c) - \lambda \mathcal{L}(\theta_a) - (1 - \lambda) \mathcal{L}(\pi(\theta_b))) \\ &= \max_{\lambda} (\lambda (\mathcal{L}(\theta_c) - \mathcal{L}(\theta_a)) + (1 - \lambda) (\mathcal{L}(\theta_c) - \mathcal{L}(\pi(\theta_b)))) \\ &= \max_{\lambda} \left( \beta \lambda (1 - \lambda) \mu^\top (\nabla \mathcal{L}(\theta_a) - \nabla \mathcal{L}(\pi(\theta_b))) + \frac{1}{2} \beta^2 \lambda (1 - \lambda) \mu^\top ((1 - \lambda) \mathbf{H}_a + \lambda \mathbf{H}_b) \mu \right) + O(\beta^3). \end{aligned}$$

□

## B.2. Proof of Theorem 4.1

*Proof.* Consider the  $L_2$  norm of the  $\ell$ -th layer  $\|\mathbf{W}_\ell^{(a)} - \mathbf{P}_\ell \mathbf{W}_\ell^{(b)} \mathbf{P}_{\ell-1}^\top\|^2$ . Using the fact that the  $L_2$  norm can be rewritten using trace, we have

$$\begin{aligned} \|\mathbf{W}_\ell^{(a)} - \mathbf{P}_\ell \mathbf{W}_\ell^{(b)} \mathbf{P}_{\ell-1}^\top\|^2 &= \text{tr} \left( (\mathbf{W}_\ell^{(a)} - \mathbf{P}_\ell \mathbf{W}_\ell^{(b)} \mathbf{P}_{\ell-1}^\top) (\mathbf{W}_\ell^{(a)} - \mathbf{P}_\ell \mathbf{W}_\ell^{(b)} \mathbf{P}_{\ell-1}^\top)^\top \right) \\ &= \text{tr} \left( \mathbf{W}_\ell^{(a)} (\mathbf{W}_\ell^{(a)})^\top \right) + \text{tr} \left( \mathbf{W}_\ell^{(b)} (\mathbf{W}_\ell^{(b)})^\top \right) - 2 \text{tr} \left( \mathbf{P}_\ell \mathbf{W}_\ell^{(b)} \mathbf{P}_{\ell-1}^\top (\mathbf{W}_\ell^{(a)})^\top \right). \end{aligned} \quad (8)$$

We focus on the last term because only it depends on the permutation matrices. The SVDs of the weights  $\mathbf{W}_\ell^{(a)}$  and  $\mathbf{W}_\ell^{(b)}$  are denoted by  $\mathbf{W}_\ell^{(a)} = \mathbf{U}_\ell^{(a)} \mathbf{S}_\ell^{(a)} (\mathbf{V}_\ell^{(a)})^\top = \sum_i \mathbf{u}_{\ell,i}^{(a)} s_{\ell,i}^{(a)} (\mathbf{v}_{\ell,i}^{(a)})^\top$  and  $\mathbf{W}_\ell^{(b)} = \mathbf{U}_\ell^{(b)} \mathbf{S}_\ell^{(b)} (\mathbf{V}_\ell^{(b)})^\top = \sum_j \mathbf{u}_{\ell,j}^{(b)} s_{\ell,j}^{(b)} (\mathbf{v}_{\ell,j}^{(b)})^\top$ , respectively. Thus, the last term of Equation (8) can be rewritten as

$$-2 \text{tr} \left( \mathbf{P}_\ell \mathbf{W}_\ell^{(b)} \mathbf{P}_{\ell-1}^\top (\mathbf{W}_\ell^{(a)})^\top \right) = -2 \sum_{i,j} s_{\ell,i}^{(a)} s_{\ell,j}^{(b)} (\mathbf{u}_{\ell,i}^{(a)})^\top (\mathbf{P}_\ell \mathbf{u}_{\ell,j}^{(b)}) (\mathbf{v}_{\ell,i}^{(a)})^\top (\mathbf{P}_{\ell-1} \mathbf{v}_{\ell,j}^{(b)}).$$

Therefore, Equation (1) equals

$$\arg \min_{\pi} \|\theta_a - \pi(\theta_b)\|^2 = \arg \max_{\pi=(\mathbf{P}_\ell)_\ell} \sum_{\ell,i,j} s_{\ell,i}^{(a)} s_{\ell,j}^{(b)} (\mathbf{u}_{\ell,i}^{(a)})^\top (\mathbf{P}_\ell \mathbf{u}_{\ell,j}^{(b)}) (\mathbf{v}_{\ell,i}^{(a)})^\top (\mathbf{P}_{\ell-1} \mathbf{v}_{\ell,j}^{(b)}),$$

which completes the proof.  $\square$

## B.3. Proof of Theorem A.1

*Proof.* Note that the matrix  $\mathbf{L}$  can be decomposed to  $\mathbf{L} = \sum_w \mathbf{G}_{:, :, w} \otimes (\mathbf{e}_w \mathbf{e}_w^\top)$  by using the tensor  $\mathbf{G}$ , where  $\mathbf{e}_w$  is the orthonormal basis in Euclidean space  $\mathbf{R}^{n^2}$ . Thus, the SVD of  $\mathbf{L}$  is given by

$$\begin{aligned} \mathbf{L} &= \sum_w \sum_i (\mathbf{u}_{w,i} \otimes \mathbf{Q}) s_{w,i} (\mathbf{v}_{w,i} \otimes \mathbf{Q})^* \otimes (\mathbf{e}_w \mathbf{e}_w^\top) \\ &= \sum_w \sum_i s_{w,i} (\mathbf{u}_{w,i} \mathbf{v}_{w,i}^*) \otimes (\mathbf{e}_w \mathbf{e}_w^\top) \\ &= \sum_w \sum_i s_{w,i} (\mathbf{u}_{w,i} \otimes \mathbf{e}_w) (\mathbf{v}_{w,i} \otimes \mathbf{e}_w)^*. \end{aligned}$$

Thus, the SVD of  $\mathbf{M}$  is also given by

$$\mathbf{M} = \sum_w \sum_i s_{w,i} (\mathbf{I}_m \otimes \mathbf{Q}) (\mathbf{u}_{w,i} \otimes \mathbf{e}_w) (\mathbf{v}_{w,i} \otimes \mathbf{e}_w)^* (\mathbf{I}_m \otimes \mathbf{Q})^* = \sum_w \sum_i s_{w,i} (\mathbf{u}_{w,i} \otimes \mathbf{Q} \mathbf{e}_w) (\mathbf{v}_{w,i} \otimes \mathbf{Q} \mathbf{e}_w)^*,$$

which completes the proof.  $\square$

## B.4. Proof of Theorem A.2

Before proving Theorem A.2, we first prove the following lemma:

**Lemma B.1.** *Let  $\mathbf{K}$  and  $\mathbf{K}'$  be kernels of a convolutional layer. We have  $\|\mathbf{M} - \mathbf{M}'\|^2 = n^2 \|\mathbf{K} - \mathbf{K}'\|^2$ , where  $\mathbf{M}$  and  $\mathbf{M}'$  are the matrix representations of  $\mathbf{K}$  and  $\mathbf{K}'$ , respectively.*

*Proof.* From the definition of  $\mathbf{M}$  and  $\mathbf{M}'$ , we have

$$\mathbf{M} = \begin{pmatrix} \mathbf{B}_{1,1} & \mathbf{B}_{1,2} & \cdots & \mathbf{B}_{1,m} \\ \mathbf{B}_{2,1} & \mathbf{B}_{2,2} & \cdots & \mathbf{B}_{2,m} \\ \vdots & \vdots & \ddots & \vdots \\ \mathbf{B}_{m,1} & \mathbf{B}_{m,2} & \cdots & \mathbf{B}_{m,m} \end{pmatrix}, \quad \mathbf{M}' = \begin{pmatrix} \mathbf{B}'_{1,1} & \mathbf{B}'_{1,2} & \cdots & \mathbf{B}'_{1,m} \\ \mathbf{B}'_{2,1} & \mathbf{B}'_{2,2} & \cdots & \mathbf{B}'_{2,m} \\ \vdots & \vdots & \ddots & \vdots \\ \mathbf{B}'_{m,1} & \mathbf{B}'_{m,2} & \cdots & \mathbf{B}'_{m,m} \end{pmatrix},$$

where for any  $c, d \in [m]$ ,  $\mathbf{B}_{c,d}$  and  $\mathbf{B}'_{c,d}$  denote the doubly circulant matrices obtained from the kernels  $\mathbf{K}$  and  $\mathbf{K}'$ . Thus,  $\|\mathbf{M} - \mathbf{M}'\|^2 = \sum_{c,d} \|\mathbf{B}_{c,d} - \mathbf{B}'_{c,d}\|^2 = n \sum_{c,d} \sum_i \|\text{circ}(\mathbf{K}_{i, :, c, d}) - \text{circ}(\mathbf{K}'_{i, :, c, d})\|^2 = n^2 \sum_{c,d} \sum_{i,j} (\mathbf{K}_{i, j, c, d} - \mathbf{K}'_{i, j, c, d})^2 = n^2 \|\mathbf{K} - \mathbf{K}'\|^2$  holds.  $\square$

*Proof of Theorem A.2.* In convolutional layers, permutation matrices permute the input and output channels of the kernel. Therefore, the permutation matrices  $P_\ell$  and  $P_{\ell-1}$  corresponding to the input and output are  $m \times m$  matrices. By using these matrices, the permutation of the matrix representation of the convolutional layer of the model  $\theta_b$  is denoted by  $(P_\ell \otimes I_m)M^{(b)}(P_{\ell-1} \otimes I_m)^\top$ . Lemma B.1 indicates that finding the permutation matrices that minimize the  $L_2$  distance between the two kernels is equivalent to minimizing  $\|M^{(a)} - (P_\ell \otimes I_m)M^{(b)}(P_{\ell-1} \otimes I_m)^\top\|$ . Therefore, we have

$$\begin{aligned} & \|M^{(a)} - (P_\ell \otimes I_m)M^{(b)}(P_{\ell-1} \otimes I_m)^\top\|^2 \\ &= \text{tr} \left( \left( M^{(a)} - (P_\ell \otimes I_m)M^{(b)}(P_{\ell-1} \otimes I_m)^\top \right) \left( M^{(a)} - (P_\ell \otimes I_m)M^{(b)}(P_{\ell-1} \otimes I_m)^\top \right)^* \right) \\ &= \text{tr} \left( M^{(a)}(M^{(a)})^\top \right) + \text{tr} \left( M^{(b)}(M^{(b)})^\top \right) - \text{tr} \left( M^{(a)} \left( (P_\ell \otimes I_m)M^{(b)}(P_{\ell-1} \otimes I_m)^\top \right)^* \right) \\ &\quad - \text{tr} \left( (P_\ell \otimes I_m)M^{(b)}(P_{\ell-1} \otimes I_m)^\top (M^{(a)})^* \right). \end{aligned} \quad (9)$$

In Equation (9), the permutation matrices  $P_\ell$  and  $P_{\ell-1}$  are only related to the last two terms. Therefore, we focus only on them. By using some properties of trace, we have

$$\begin{aligned} & -\text{tr} \left( M^{(a)} \left( (P_\ell \otimes I_m)M^{(b)}(P_{\ell-1} \otimes I_m)^\top \right)^* \right) - \text{tr} \left( (P_\ell \otimes I_m)M^{(b)}(P_{\ell-1} \otimes I_m)^\top (M^{(a)})^* \right) \\ &= -\text{tr} \left( M^{(a)} \left( (P_\ell \otimes I_m)M^{(b)}(P_{\ell-1} \otimes I_m)^\top \right)^* \right) - \text{tr} \left( \left( M^{(a)} \left( (P_\ell \otimes I_m)M^{(b)}(P_{\ell-1} \otimes I_m)^\top \right)^* \right)^* \right) \\ &= -\text{tr} \left( M^{(a)} \left( (P_\ell \otimes I_m)M^{(b)}(P_{\ell-1} \otimes I_m)^\top \right)^* \right) - \overline{\text{tr} \left( M^{(a)} \left( (P_\ell \otimes I_m)M^{(b)}(P_{\ell-1} \otimes I_m)^\top \right)^* \right)} \\ &= -2\Re \text{tr} \left( M^{(a)} \left( (P_\ell \otimes I_m)M^{(b)}(P_{\ell-1} \otimes I_m)^\top \right)^* \right). \end{aligned}$$

Here, from Theorem A.1,

$$M^{(a)} = \sum_{w,i} (\mathbf{u}_{w,i}^{(a)} \otimes \mathbf{Q}e_w) s_{w,i}^{(a)} (\mathbf{v}_{w,i}^{(a)} \otimes \mathbf{Q}e_w)^* = \sum_{w,i} s_{w,i}^{(a)} (\mathbf{u}_{w,i}^{(a)} (\mathbf{v}_{w,i}^{(a)})^* \otimes \mathbf{Q}e_w e_w^\top \mathbf{Q}^*) = \sum_w (C_w^{(a)} \otimes \mathbf{Q}e_w e_w^\top \mathbf{Q}^*), \quad (10)$$

and

$$\begin{aligned} (P_\ell \otimes I_m)M^{(b)}(P_{\ell-1} \otimes I_m)^\top &= \sum_{w,i} s_{w,i}^{(b)} (P_\ell \otimes I_m) (\mathbf{u}_{w,i}^{(b)} \otimes \mathbf{Q}e_w) (\mathbf{v}_{w,i}^{(b)} \otimes \mathbf{Q}e_w)^* (P_{\ell-1} \otimes I_m)^\top \\ &= \sum_{w,i} s_{w,i}^{(b)} (P_\ell \mathbf{u}_{w,i}^{(b)} (P_{\ell-1} \mathbf{v}_{w,i}^{(b)})^* \otimes \mathbf{Q}e_w e_w^\top \mathbf{Q}^*) \\ &= \sum_w (C_w^{(b)} \otimes \mathbf{Q}e_w e_w^\top \mathbf{Q}^*) \end{aligned} \quad (11)$$

holds, where we let  $C_w^{(a)} = \sum_i s_{w,i}^{(a)} \mathbf{u}_{w,i}^{(a)} (\mathbf{v}_{w,i}^{(a)})^*$  and  $C_w^{(b)} = \sum_i s_{w,i}^{(b)} (P_\ell \mathbf{u}_{w,i}^{(b)}) (P_{\ell-1} \mathbf{v}_{w,i}^{(b)})^*$ . From Equation (10) and Equation (11), we have

$$\begin{aligned} & -2\Re \text{tr} \left( M^{(a)} \left( (P_\ell \otimes I_m)M^{(b)}(P_{\ell-1} \otimes I_m)^\top \right)^* \right) \\ &= -2\Re \text{tr} \left( \sum_w (C_w^{(a)} \otimes \mathbf{Q}e_w e_w^\top \mathbf{Q}^*) \left( \sum_{w'} (C_{w'}^{(b)} \otimes \mathbf{Q}e_{w'} e_{w'}^\top \mathbf{Q}^*) \right)^* \right) \\ &= -2\Re \text{tr} \left( \sum_{w,w'} \left( C_w^{(a)} (C_{w'}^{(b)})^* \otimes \mathbf{Q}e_w e_w^\top e_{w'} e_{w'}^\top \mathbf{Q}^* \right) \right). \end{aligned}$$

Using the fact that if  $w \neq w'$ , then  $e_w^\top e_{w'} = 0$ , and otherwise,  $e_w^\top e_{w'} = 1$ , we have

$$\begin{aligned}
 & -2\Re \operatorname{tr} \left( M^{(a)} \left( (P_\ell \otimes I_m) M^{(b)} (P_{\ell-1} \otimes I_m)^\top \right)^\top \right) \\
 &= -2\Re \sum_w \operatorname{tr} \left( C_w^{(a)} (C_w^{(b)})^* \otimes Q e_w e_w^\top Q^* \right) \\
 &= -2\Re \sum_w \operatorname{tr} \left( C_w^{(a)} (C_w^{(b)})^* \right) \operatorname{tr} (Q e_w e_w^\top Q^*) \\
 &= -2\Re \sum_w \operatorname{tr} \left( C_w^{(a)} (C_w^{(b)})^* \right) \\
 &= -2\Re \sum_w \operatorname{tr} \left( \left( \sum_i s_{w,i}^{(a)} \mathbf{u}_{w,i}^{(a)} (\mathbf{v}_{w,i}^{(a)})^* \right) \left( \sum_j s_{w,j}^{(b)} (P_\ell \mathbf{u}_{w,j}^{(b)}) (P_{\ell-1} \mathbf{v}_{w,j}^{(b)})^* \right)^\top \right) \\
 &= -2\Re \sum_w \sum_{i,j} s_{w,i}^{(a)} s_{w,j}^{(b)} \left( (\mathbf{u}_{w,i}^{(a)})^* (P_\ell \mathbf{u}_{w,j}^{(b)}) \right)^* \left( (\mathbf{v}_{w,i}^{(a)})^* (P_{\ell-1} \mathbf{v}_{w,j}^{(b)}) \right).
 \end{aligned}$$

From the above, the minimization of  $\|M^{(a)} - (P_\ell \otimes I_m) M^{(b)} (P_{\ell-1} \otimes I_m)^\top\|$  is equivalent to the maximization of  $\Re \sum_w \sum_{i,j} s_{w,i}^{(a)} s_{w,j}^{(b)} \left( (\mathbf{u}_{w,i}^{(a)})^* (P_\ell \mathbf{u}_{w,j}^{(b)}) \right)^* \left( (\mathbf{v}_{w,i}^{(a)})^* (P_{\ell-1} \mathbf{v}_{w,j}^{(b)}) \right)$ .  $\square$

### B.5. Proof of $|R(\theta_a, \pi(\theta_b))| \leq 1$

This subsection proves the following theorem:

**Theorem B.2.** Let  $\theta_a$  and  $\theta_b$  be the parameters of two MLPs with  $L$ -layers. For any permutation  $\pi = (P_\ell)_{\ell \in [L]}$ , we have

$$|R(\theta_a, \pi(\theta_b))| = \frac{\left| \sum_{\ell,i,j} (\mathbf{u}_{\ell,i}^{(a)})^\top (P_\ell \mathbf{u}_{\ell,j}^{(b)}) (\mathbf{v}_{\ell,i}^{(a)})^\top (P_{\ell-1} \mathbf{v}_{\ell,j}^{(b)}) \right|}{\sum_\ell n_\ell} \leq 1. \quad (12)$$

The equality holds if, for all  $\ell, i$ ,  $\mathbf{u}_{\ell,i}^{(a)} = P_\ell \mathbf{u}_{\ell,i}^{(b)}$  and  $\mathbf{v}_{\ell,i}^{(a)} = P_{\ell-1} \mathbf{v}_{\ell,i}^{(b)}$ .

*Proof.* If, for all  $\ell, i$ ,  $\mathbf{u}_{\ell,i}^{(a)} = P_\ell \mathbf{u}_{\ell,i}^{(b)}$  and  $\mathbf{v}_{\ell,i}^{(a)} = P_{\ell-1} \mathbf{v}_{\ell,i}^{(b)}$ , the equality obviously holds. Thus, we prove that Equation (12) holds. Using the property of trace, we have

$$\begin{aligned}
 \sum_{\ell,i,j} (\mathbf{u}_{\ell,i}^{(a)})^\top (P_\ell \mathbf{u}_{\ell,j}^{(b)}) (\mathbf{v}_{\ell,i}^{(a)})^\top (P_{\ell-1} \mathbf{v}_{\ell,j}^{(b)}) &= \sum_{\ell,i,j} (P_\ell \mathbf{u}_{\ell,j}^{(b)})^\top (\mathbf{u}_{\ell,i}^{(a)}) (\mathbf{v}_{\ell,i}^{(a)})^\top (P_{\ell-1} \mathbf{v}_{\ell,j}^{(b)}) \\
 &= \sum_\ell \operatorname{tr} \left( \sum_i (\mathbf{u}_{\ell,i}^{(a)}) (\mathbf{v}_{\ell,i}^{(a)})^\top \sum_j \left( (P_\ell \mathbf{u}_{\ell,j}^{(b)}) (P_{\ell-1} \mathbf{v}_{\ell,j}^{(b)})^\top \right)^\top \right).
 \end{aligned}$$

Let  $\mathbf{W}_\ell'^{(a)} = \sum_i (\mathbf{u}_{\ell,i}^{(a)}) (\mathbf{v}_{\ell,i}^{(a)})^\top$  and  $\mathbf{W}_\ell'^{(b)} = \sum_j (P_\ell \mathbf{u}_{\ell,j}^{(b)}) (P_{\ell-1} \mathbf{v}_{\ell,j}^{(b)})^\top$ . Obviously, they are matrices with all singular values of 1, and thus by using von Neuman's trace inequality (von Neumann, 1962), we have

$$\sum_\ell \left| \operatorname{tr} \left( \mathbf{W}_\ell'^{(b)} (\mathbf{W}_\ell'^{(a)})^\top \right) \right| \leq \sum_\ell n_\ell.$$

Therefore, the triangle inequality yields that

$$\sum_{\ell,i,j} (\mathbf{u}_{\ell,i}^{(a)})^\top (P_\ell \mathbf{u}_{\ell,j}^{(b)}) (\mathbf{v}_{\ell,i}^{(a)})^\top (P_{\ell-1} \mathbf{v}_{\ell,j}^{(b)}) = \left| \sum_\ell \operatorname{tr} \left( \mathbf{W}_\ell'^{(b)} (\mathbf{W}_\ell'^{(a)})^\top \right) \right| \leq \sum_\ell \left| \operatorname{tr} \left( \mathbf{W}_\ell'^{(b)} (\mathbf{W}_\ell'^{(a)})^\top \right) \right| \leq \sum_\ell n_\ell,$$

which completes the proof.  $\square$



Table 3. Evaluation results of barrier and R values between each pair of models

	Dataset	Network	Accuracy barrier			Loss barrier			R value		
			$(\theta_a + \pi_b(\theta_b))/2$	$(\theta_a + \pi_c(\theta_c))/2$	$(\pi_b(\theta_b) + \pi_c(\theta_c))/2$	$(\theta_a + \pi_b(\theta_b))/2$	$(\theta_a + \pi_c(\theta_c))/2$	$(\pi_b(\theta_b) + \pi_c(\theta_c))/2$	$R(\theta_a, \pi_b(\theta_b))$	$R(\theta_a, \pi_c(\theta_c))$	$R(\pi_b(\theta_b), \pi_c(\theta_c))$
WM	CIFAR10	VGG11	0.094 ± 0.158	0.037 ± 0.156	0.141 ± 0.141	8.362 ± 5.677	7.555 ± 4.978	10.12 ± 5.117	0.199 ± 0.042	0.195 ± 0.027	0.1 ± 0.015
		ResNet20	0.135 ± 0.026	0.098 ± 0.011	0.294 ± 0.098	3.312 ± 0.61	2.995 ± 0.064	7.23 ± 0.99	0.23 ± 0.016	0.211 ± 0.008	0.102 ± 0.005
	FMNIST	MLP	-0.211 ± 0.029	-0.174 ± 0.044	-0.174 ± 0.051	1.947 ± 0.501	1.703 ± 0.289	4.337 ± 1.434	0.335 ± 0.003	0.334 ± 0.002	0.209 ± 0.003
		MNIST	MLP	-0.027 ± 0.005	-0.034 ± 0.003	-0.031 ± 0.003	0.173 ± 0.04	0.198 ± 0.032	0.475 ± 0.069	0.421 ± 0.009	0.425 ± 0.006
STE	CIFAR10	VGG11	0.081 ± 0.031	0.099 ± 0.042	2.172 ± 0.989	4.86 ± 0.815	5.76 ± 0.537	32.013 ± 8.193	0.01 ± 0.001	0.01 ± 0.001	0.019 ± 0.002
		ResNet20	0.466 ± 0.154	0.446 ± 0.138	1.693 ± 0.168	15.005 ± 3.765	13.942 ± 4.008	34.483 ± 2.426	0.008 ± 0.004	0.007 ± 0.003	0.02 ± 0.004
	FMNIST	MLP	-0.372 ± 0.016	-0.343 ± 0.055	0.023 ± 0.118	2.667 ± 0.248	2.483 ± 0.621	15.97 ± 1.724	0.073 ± 0.002	0.081 ± 0.009	0.047 ± 0.002
		MNIST	MLP	-0.037 ± 0.011	-0.039 ± 0.006	0.017 ± 0.014	0.253 ± 0.176	0.358 ± 0.198	2.312 ± 0.457	0.201 ± 0.019	0.203 ± 0.007

## C. Experimental Setup

We describe the experimental setup for training neural networks to obtain SGD solutions. In this work, we apply Sinkhorn’s algorithm for permutation based on WM and STE. Thus, we also detail the experimental setup for Sinkhorn’s algorithm.

In our paper, all experiments were conducted on a Linux workstation with two AMD EPYC 7543 32-Core processors, eight NVIDIA A30 GPUs, and 512 GB memory.

### C.1. Model Training

**MLP on MNIST and FMNIST.** Following the settings in (Ainsworth et al., 2023), we train a Multi-Layer Perceptron (MLP) with three hidden layers, each comprising 512 units. The intermediate layers employ the ReLU function as their activation function. For MNIST and FMNIST datasets, we optimize using the Adam algorithm with a learning rate of  $1 \times 10^{-3}$ .

**VGG11 and ResNet20 on CIFAR10.** To accomplish Layer-wise Model Compression (LMC), we increase the widths of VGG11 and ResNet20 by factors of 4 and 16, respectively. As described in (Jordan et al., 2023), we repair the BatchNorm layers in these models during model merging by using the training dataset. Optimization is conducted using Adam with a learning rate of  $1 \times 10^{-3}$ .

### C.2. Permutation Search

For permutation search in this study, we employ the method based on Sinkhorn’s algorithm as proposed by Peña et al. (2023). We utilize the implementation provided by the authors in their GitHub repository<sup>5</sup>. DistL2Loss and MidLoss are used as loss functions for permutation searches corresponding to WM and STE, respectively. Optimization for all models is performed using Adam with a learning rate of 1, setting the maximum number of epochs to ten for DistL2Loss and five for MidLoss.

## D. Additional Results

### D.1. Experimental Results of STE and WM

In this section, additional experimental results for Section 5.3 are shown in Table 3 for the barrier values and  $R$  values between each pair of models. The table shows the model-merging results with  $\lambda = 1/2$ , and the mean and standard deviation of five model merges. In the table, a negative value for the barrier indicates an improvement in performance due to the merging. From the Table 3, we can see that the barrier between  $\pi_b(\theta_b)$  and  $\pi_c(\theta_c)$  is also smaller for WM than for STE.

### D.2. Distribution of Singular Values

Figure 6 shows the distribution of the singular values of all the layers. The figure shows in the intermediate layers, the singular values are very close across all models. Meanwhile, in the final layers, there is variability in the singular values. Note that this variability does not affect the accuracy values for the merged model. Let  $\mathbf{W}_L^{(a)} = \sum_i s_{L,i}^{(a)} \mathbf{u}_{L,i}^{(a)} (\mathbf{v}^{(a)})_{L,i}^\top$  and  $\mathbf{W}_L^{(b)} = \sum_i s_{L,i}^{(b)} \mathbf{u}_{L,i}^{(b)} (\mathbf{v}^{(b)})_{L,i}^\top$  be the final layer weights of the two trained models. The figure shows that the difference between the singular values of the two models is approximately a constant multiple. In other words, there exists a constant  $\alpha$  and  $s_{L,i}^{(a)} \approx \alpha s_{L,i}^{(b)}$  for all  $i$ . Then, if the singular vectors of the two weights are equal (i.e.,  $\mathbf{v}_{L,i}^{(a)} = \mathbf{v}_{L,i}^{(b)}$  and  $\mathbf{u}_{L,i}^{(a)} = \mathbf{u}_{L,i}^{(b)}$

<sup>5</sup><https://github.com/fagp/sinkhorn-rebasin>

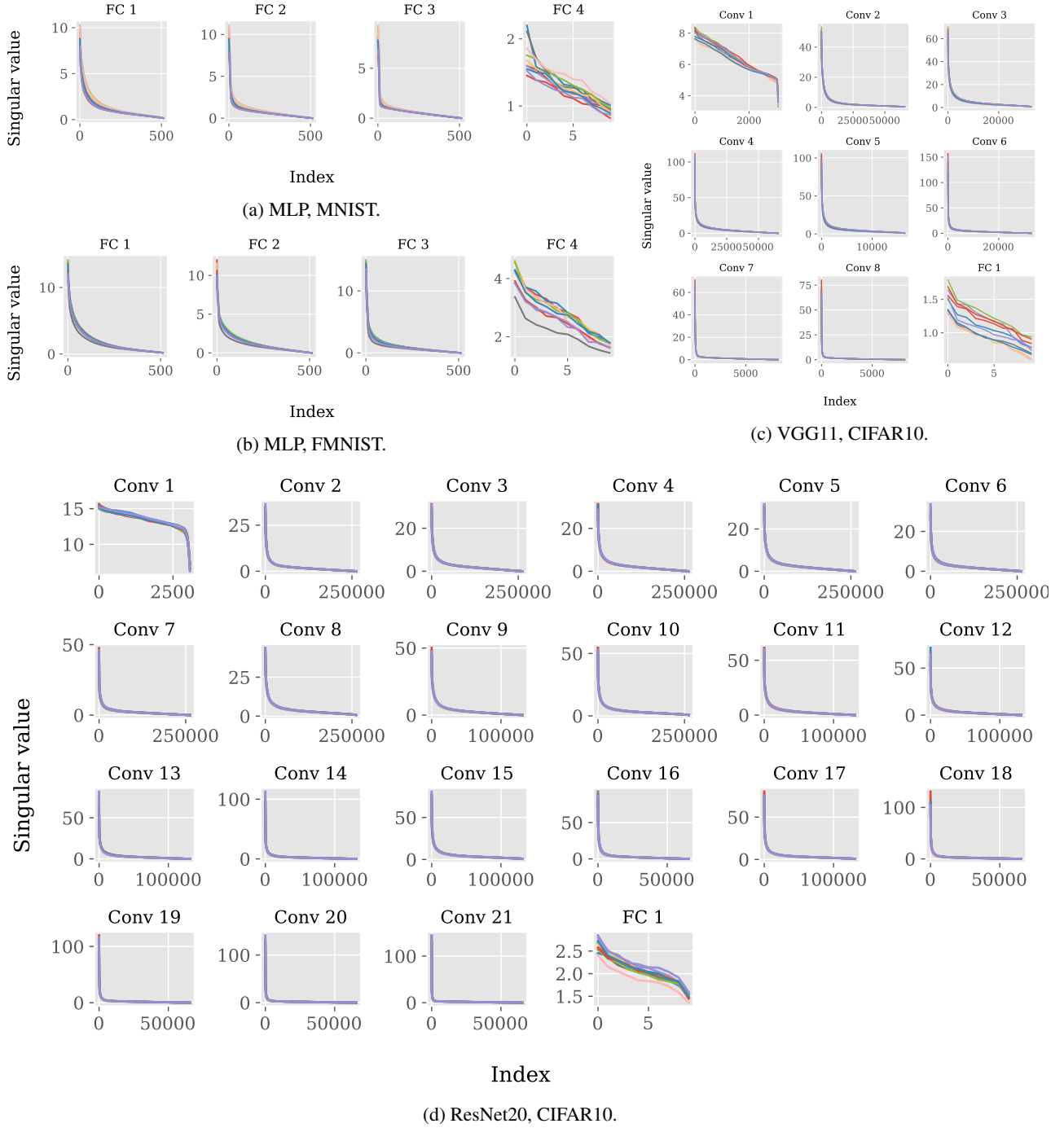


Figure 6. Distribution of the singular values of each layer.

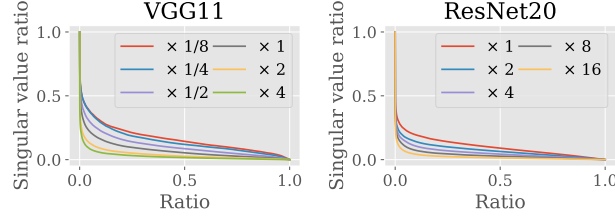
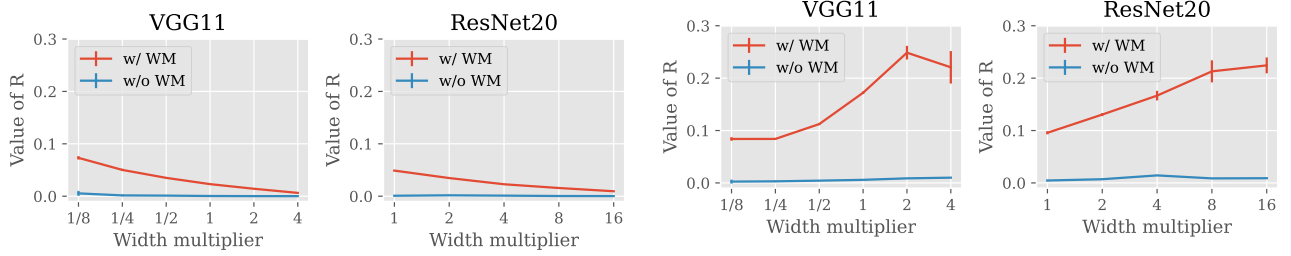


Figure 7. Distribution of singular values as the multiplier of the model width changes.



(a) Evaluation results of Equation (5) for all the singular vectors.

 (b) Evaluation results of Equation (5) for the singular vectors with  $\gamma = 0.3$ .

Figure 8. Relation between the model width and the difficulty in aligning the directions of singular vectors.

for all  $i$ ), then  $\mathbf{W}_L^{(a)} \approx \alpha \mathbf{W}_L^{(b)}$  holds (indeed, as mentioned in Section 4.3, the permutation matrix brings the directions of the singular vectors close). Therefore, the weight of the final layer of the merged model at the ratio  $\lambda \in [0, 1]$  is given by  $\lambda \mathbf{W}_L^{(a)} + (1 - \lambda) \mathbf{W}_L^{(b)} \approx \lambda \mathbf{W}_L^{(a)} + (1 - \lambda) \alpha \mathbf{W}_L^{(a)} = (\lambda + (1 - \lambda) \alpha) \mathbf{W}_L^{(a)}$ . Thus, we can consider that the weight and activation function of the merged model are given by  $\mathbf{W}_L^{(a)}$  and a softmax function with an inverse temperature of  $1/(\lambda + (1 - \lambda) \alpha)$ . Since the inverse temperature does not affect the accuracy value, the difference in the singular values of the final layer would not matter in satisfying the LMC, at least in terms of accuracy value.

### D.3. Relationship with Model Width

Previous studies have demonstrated that the width of the model architecture affects the ease of achieving LMC. In this section, we explain this reason from the following two facts: (i) the proportion of dominant singular values decreases as the model width increases, and (ii) the WM preferentially aligns the directions of singular vectors corresponding to such dominant singular values.

**Relationship between Model Width and Distribution of Singular Values.** As we mentioned, the proportion of relatively large singular values in all singular values decreases as the model width increases. To verify this, Figure 7 shows the distribution of the singular values of all layers of VGG11 and ResNet20 trained on CIFAR10. Figure 7 shows the results of different model widths (i.e., dimensionality). The vertical axis represents the singular values divided by the maximum singular value of each model, and the horizontal axis represents the ratio among all singular values (e.g., the point at 0.5 on the horizontal axis represents the singular value in the middle of all values sorted in descending order). As can be seen, the proportion of relatively large singular values decreases as the model width increases. Thus, the proportion of singular vectors that need to be aligned in the model decreases as width increases, suggesting that wider models make it easier to satisfy LMC by WM.

**Singular-Vector Alignment** We conduct an experiment to examine how well the directions of singular vectors are aligned as the model width is increased when the permutations found by the WM are applied. The results are shown in Figure 8. The figures show the results of evaluating  $R(\theta_a, \pi(\theta_b))$  for the trained models  $\theta_a$  and  $\theta_b$  by searching permutations  $\pi$  so that  $\theta_b$  approaches  $\theta_a$  by WM. For comparison, the case where no permutations are applied (i.e.,  $\pi$  is an identity map) is also shown. A threshold  $\gamma$  was also introduced to evaluate how well the directions of the singular vectors with large singular values are

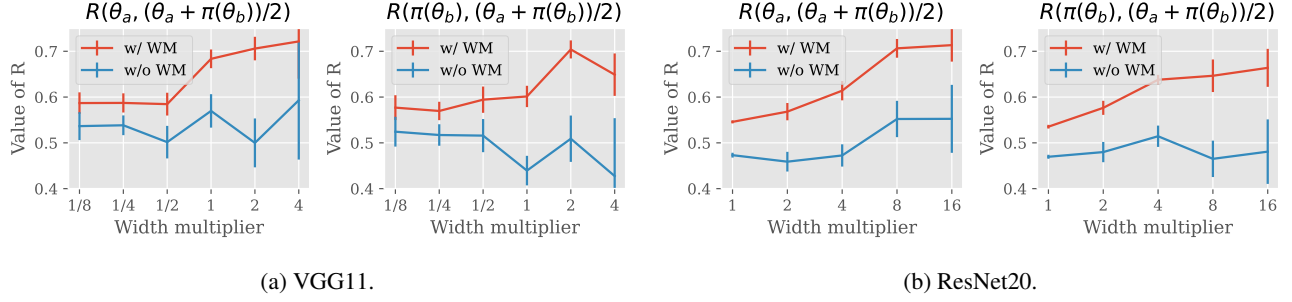


Figure 9. Relation between the model width and the difficulty in aligning the directions of singular vectors.

aligned. First, focusing on the results for Figure 8(a) with  $\gamma = 0$ , we can see that the value of  $R$  decreases even when the width increases and WM is used. On the other hand, the Figure 8(b) shows that the directions of the singular vectors with particularly large singular values are aligned by permutation when the model width is increased. This indicates that even with WM, it is difficult to perfectly align the directions of singular vectors between the two models, while increasing the width decreases the fraction of singular vectors with large singular values, and thus WM attempts to align the directions of such dominant singular vectors.

To investigate the impact of this alignment on the singular vectors of the merged model, we evaluate how well the singular vectors of the model are aligned before and after merging, and the results are shown in Figure 9. In the figures, the value of the function  $R$  is evaluated with  $\gamma = 0.3$  in order to focus on the singular vectors with large singular values. Figure 9 shows that as the model width increases, the singular vectors' directions with large singular values are aligned between the models before and after merging. Considering that the input-output relationship of each model layer is determined by the singular vector with the large singular value, this figure indicates that by increasing the model width, the function of the merged model approaches the models  $\theta_a$  and  $\theta_b$ . Therefore, increasing the width is expected to make the LMC more feasible.

## E. Limitations

Our analysis in this paper has some limitations. In this paper, we have explained LMCs by WM in terms of SVD for the weights of each layer, but this does not explain why all LMCs occur. For example, STE, which directly searches for permutations that reduce the barrier, does not align the directions of singular vectors, so the method of analysis in this paper cannot explain why STE can achieve LMC. In addition, the analysis in this paper can only be applied to image classification tasks using the same dataset. The applicability to different datasets and image generation tasks is a subject for future work.